AGU ADVANCING EARTH AND SPACE SCIENCE

Earth and Space Science

RESEARCH ARTICLE
10.1029/2022EA002733

A Comparative Study Between Regional Atmospheric Model Simulations Coupled and Uncoupled to a Regional Ocean Model of the Indian Summer Monsoon

C. B. Jayasankar[1,2], Vasubandhu Misra[1,2,3], and Nirupam Karmakar[4,5,6]

[1]Center for Ocean-Atmospheric Prediction Studies, Florida State University, Tallahassee, FL, USA, [2]Florida Climate Institute, Florida State University, Tallahassee, FL, USA, [3]Department of Earth, Ocean and Atmospheric Science, Florida State University, Tallahassee, FL, USA, [4]Indian Institute of Tropical Meteorology, Pune, India, [5]National Centre for Medium Range Weather Forecasting (MoES), Noida, India, [6]School of Earth, Ocean and Climate Sciences, Indian Institute of Technology Bhubaneswar, Odisha, India

Key Points:

- Air-sea coupling in dynamically downscaled simulation improves the mean Indian summer monsoon relative to the parent general circulation models (GCM) simulation
- Coupled ocean-atmosphere and atmosphere-only regional climate models (RCMs) simulate intraseasonal oscillations (ISOs) of the monsoon with only subtle differences
- RCMs add value to downscaling by simulating realistic intraseasonal variability of the monsoon low-pressure systems absent in the parent GCM

Supporting Information:

Supporting Information may be found in the online version of this article.

Correspondence to:

C. B. Jayasankar,
cbjayasankar@gmail.com;
jcb@fsu.edu

Citation:

Jayasankar, C. B., Misra, V., & Karmakar, N. (2023). A comparative study between regional atmospheric model simulations coupled and uncoupled to a regional ocean model of the Indian summer monsoon. *Earth and Space Science*, *10*, e2022EA002733. https://doi.org/10.1029/2022EA002733

Received 13 NOV 2022
Accepted 14 MAR 2023

Author Contributions:

Conceptualization: C. B. Jayasankar, Vasubandhu Misra
Data curation: C. B. Jayasankar, Vasubandhu Misra
Formal analysis: C. B. Jayasankar
Funding acquisition: Vasubandhu Misra

Abstract We evaluate the impact of air-sea coupling in simulating the characteristics of the Indian summer monsoon (ISM) and its intraseasonal oscillations (ISOs) by using a coupled ocean-atmosphere regional climate model (CRSM) and an atmosphere-only regional climate model (URSM). These 20-km resolution regional climate models (RCMs) were driven by the boundary conditions from Community Climate System Model version 4 (CCSM4) global model. The mean ISM rainfall simulated by URSM and CRSM is comparable with observations and shows an improvement over the CCSM4. The systematic error in the spatial distribution of the mean June–September low-level and upper-level winds, sea surface temperature, and latent heat flux shows that CRSM performs better than URSM, suggesting the benefits of air-sea coupling in the RCM simulations of the mean ISM. Both the CRSM and the URSM perform reasonably and comparably in capturing the spatiotemporal evolution of 10–20-day high-frequency and 20–70-day low-frequency ISOs of the ISM rainfall. These RCMs simulated the observed features of the ISO-filtered rainfall anomalies that propagate at a faster rate across the Arabian Sea compared to that over the Bay of Bengal. Furthermore, the difference in the track density of the monsoon low-pressure systems between the wet and the dry phases of ISOs shows insignificant differences between CRSM and URSM but is found to be superior to the CCSM4 simulation. This study suggests a relative insensitivity of air-sea coupling in the RCM for simulating ISO and LPS features of ISM, which is likely abetted by the realistic ISO signals in the parent CCSM4.

Plain Language Summary We generated two different high-resolution regional climate simulations: an atmosphere-only regional climate model (RCM) and a coupled ocean-atmosphere RCM forced with coarse-resolution global fields. By using these high-resolution regional climate simulations, we investigate how air-sea coupling affects the observed characteristics of the Indian summer monsoon (ISM) and its intraseasonal oscillations (ISOs). The results of the 20-year regional climate simulation from each of the RCMs reveal that they reasonably capture the observed mean climatology and ISOs of the ISM. The benefit of air-sea coupling in simulating the mean ISM is clear from the comparisons between the coupled and uncoupled RCM simulations. Nonetheless, the differences in the simulated characteristics of the ISO and the monsoon low-pressure systems between the RCMs were trivial. On the other hand, both the RCMs considerably outperform the global model in simulating the monsoon low-pressure systems and their association with the ISOs of the ISM. This study concludes that ISO simulation in the RCM could be insensitive to air-sea coupling because of realistic ISO signals in the driving global climate model.

1. Introduction

The Indian summer monsoon (ISM) is an important tropical coupled ocean-atmosphere system. The intraseasonal oscillations (ISOs), are one of the dominant features of the ISM (Krishnamurthy & Shukla, 2007; Sikka & Gadgil, 1980). Many studies suggest that coupled ocean-atmosphere climate models are the best tools to simulate the ISM and its variability, realistically (Goswami et al., 2016; Rajendran & Kitoh, 2006; Sharmila et al., 2013; Wang et al., 2005). Previous studies have shown that the tropical ISOs simulated by the coupled general circulation models (CGCMs) outperform the sea surface temperature (SST) forced atmospheric general circulation models (AGCMs) (Fu et al., 2002; Jiang et al., 2004; Rajendran & Kitoh, 2006; Zheng et al., 2004). For example,

Investigation: C. B. Jayasankar, Vasubandhu Misra
Methodology: C. B. Jayasankar, Vasubandhu Misra, Nirupam Karmakar
Project Administration: Vasubandhu Misra
Resources: Vasubandhu Misra
Software: C. B. Jayasankar, Nirupam Karmakar
Supervision: Vasubandhu Misra
Validation: C. B. Jayasankar
Visualization: C. B. Jayasankar
Writing – original draft: C. B. Jayasankar, Vasubandhu Misra, Nirupam Karmakar
Writing – review & editing: C. B. Jayasankar, Vasubandhu Misra, Nirupam Karmakar

Fu et al. (2002) show that air-sea coupling improved the simulation of mean ISM rainfall and the meridional propagation of ISOs. Zheng et al. (2004) found considerable disparities between the CGCM and AGCM simulations in their phase relationships between ISO anomalies of rainfall and SST. They showed that in the AGCM, rainfall lags SST by around 8 days, compared to 15 days in observations and in the CGCM. Furthermore, AGCMs are also found to exacerbate the bias in ISO amplitude, phase, and life cycle relative to the CGCM (Rajendran & Kitoh, 2006).

The majority of the CGCMs demonstrate reasonable skill in simulating the seasonal mean rainfall over the ISM region, but they exhibit weak intraseasonal variance (Lin et al., 2008). For example, Peatman and Klingaman (2018) found that the MetUM-GOML2.0 showed very low intraseasonal (24–70 days) variance across the Indian region. They found that this coupled model could simulate a realistic northward propagation of the ISO across the ocean, but it ceased over land, barely producing any rainfall over India. In contrast, Valdivieso et al. (2021) showed little impact of air-sea coupling on the numerical weather prediction of ISM rainfall. Most current global CGCMs are relatively coarse in horizontal resolution, typically a few hundred kilometers or more in grid spacing. Due to their coarse resolution, these models face difficulties in simulating the subgrid-scale processes and frequently fail to capture the small-scale regional features. Dynamical downscaling of coarse-resolution global general circulation models (GCM) through high-resolution regional climate models (RCMs) is a widely used approach to overcome horizontal resolution-dependent difficulties. RCMs are widely used to study the variabilities of the ISM (Bhaskaran et al., 1996, 2012; Dash et al., 2006; Jayasankar et al., 2018; Ji & Vernekar, 1997; Misra et al., 2018, 2022). The majority of the earlier dynamical downscaling studies relied on atmosphere-only RCMs forced with prescribed SST (Ajay et al., 2019; Befort et al., 2016; Chen et al., 2018; Dash et al., 2006; Lucas-Picher et al., 2011; Maurya et al., 2020; Mishra & Dubey, 2021; Mishra, Dubey & Dinesh, 2022; Misra et al., 2017; Pattnayak et al., 2018; Rai et al., 2020; Umakanth et al., 2016). These studies highlight the significance of the spatial resolution and especially due to improved representation of orography in high-resolution RCMs, they outperformed their forcing global GCMs in simulating the spatio-temporal distribution of the mean ISM rainfall. In addition, RCMs driven by realistic lateral boundary forcings were found to be crucial for the improved simulation of ISM (Bhaskaran et al., 2012). However, many of the RCMs overestimate the oceanic rainfall, which is likely an amplification of the global model bias (e.g., Kumar et al., 2020). For example, Kitoh and Arakawa (1999) suggest that AGCMs with prescribed SST can have stronger rainfall episodes over oceans than coupled models because they don't consider negative feedback to the ocean from the atmosphere.

The Coordinated Regional Climate Downscaling Experiments (CORDEX) Program provides ∼50-km resolution dynamically downscaled simulation for various parts of the world. CORDEX outputs were generated using different atmosphere-only RCMs, driven by Coupled Model Intercomparison Project Phase 5 (CMIP5) lateral boundary conditions with prescribed SST. Several studies utilize these downscaled simulations to study the ISM and its variabilities at different timescales (Maharana et al., 2021; Singh et al., 2017). CORDEX—South Asia models exhibit modest improvement in simulating the duration of active and break spells than their parent models; however, most of the models failed to reproduce the northward and eastward propagations of the ISOs (Singh et al., 2017).

Several studies have attempted to demonstrate the value addition of coupled ocean-atmosphere RCM over a stand-alone atmosphere RCM in simulating the ISM (Di Sante et al., 2019; Kumar, Mishra, et al., 2022; Mishra et al., 2021; Ratnam et al., 2009; Samala et al., 2013; Umakanth & Kesarkar, 2018). Samala et al. (2013) and Umakanth and Kesarkar (2018) indicate improvements in the representation of the ISO variability by a coupled RCM compared to the stand-alone atmospheric RCM. Samanta et al. (2018) and Hari Prasad et al. (2021), found that dry bias in Central India was reduced when an atmospheric RCM was coupled to an ocean mixed layer model relative to an atmosphere-only RCM. Samanta et al. (2018) suggest that the warm SST front in the Bay of Bengal (BoB) is crucial for the Central India rainfall because the realistic SST enhances the portrayal of monsoon LPSs. Using a coupled RCM, Levine et al. (2021) found that LPS simulation over the northern Indian Ocean is sensitive to localized coupling. They show that the number of LPS and the accompanying rainfall are positively impacted by air-sea coupling in the RCM. Mishra et al. (2021) found that coupled RCM represents the ISM rainfall intensity and the ISO better compared to the stand-alone atmosphere-only RCM forced with observed SST.

In the assessment of the skill of their regional earth system model (ESM) across the tropical Indian Ocean, Kumar, Mishra, et al. (2022), Kumar, Mallick, et al. (2022) found that the RCM has greater skill than its parent global GCM in representing the mean and the variability of the ISM. Also, these studies point to the major role

of air-sea coupling in lessening the wet bias compared to atmospheric RCM over south-central India and the neighboring oceans. However, they also report that the regional ESM overestimates the extreme rainfall which is attributed to the enhanced contribution from the LPS. Similarly, Mishra, Kumar, et al. (2022) showed that this regional ESM has greater skill in simulating the northward and eastward propagation of 20–100 days filtered ISO rainfall anomalies over the ocean than its stand-alone atmospheric model. But Mishra, Kumar, et al. (2022) noticed that the model had minimal improvement in the propagation characteristics of ISO anomalies over land, which they attributed to the influence of atmospheric internal dynamics in the coupled system and bias in the SST. Similarly, Di Sante et al. (2019) highlighted the importance of the air-sea coupling in the reasonable simulation of the northward propagation of convection across the Indian Ocean in another coupled RCM study.

Table 1 summarizes how different the present study is from earlier intercomparison studies between stand-alone atmospheric RCM integrations and coupled with a regional ocean model. This study stands apart in its horizontal resolution and air-sea coupling interval compared to the other studies (Table 1). However, more saliently this study differs methodologically from these earlier comparative studies. For example, in the studies by Ratnam et al. (2009) and Samala et al. (2013), the comparison is between a stand-alone atmospheric RCM forced with observed SST and a coupled version in which the regional ocean model is forced with climatological ocean fields at the lateral boundaries. Such model inter-comparison studies have very different SST forcing between the two models, which then obfuscates the response to air-sea coupling. In these studies, even if the coupled RCM is "perfect," the kind of lateral boundary forcing applied to the regional ocean model will never produce the observed SST used in the stand-alone integration. Therefore, in such studies, the impact of air-sea coupling is perceived to be significantly different from the prescribed SST RCM experiment.

Similarly, Umakant and Keskar (2018) coupled their atmospheric RCM to a slab ocean model with appropriate Q-flux correction to restore the SST to the observed SST over a 5-day period. This type of inter-comparison overlooks the impact of Q-flux correction as it tries to restore the simulated SST to be more realistic. Likewise, Di Sante et al. (2019) compare observed atmospheric RCM driven by observed SST and the coupled version of the RCM, which undermines the role of the SST bias in the latter. However, both these studies conduct additional stand-alone atmospheric RCM experiments with SST prescribed at a daily interval from the corresponding coupled ocean-atmosphere RCM integration coupled at a different interval. This comparison essentially examines the sensitivity of the air-sea coupling interval while ignoring the role of RCM bias. Under most circumstances, unless we are dealing with a "perfect" RCM, it is difficult to accurately determine the role of air-sea coupling in an RCM when it is forced with reanalysis at the lateral boundaries for the oceanic or the atmospheric components of the coupled RCM, or when observed SST is used for the stand-alone atmospheric RCM integrations. This study suggests an alternative strategy to study the "added value" of air-sea coupling in RCMs.

Our study is designed to examine if air-sea coupling included in an RCM to downscale a CGCM from the CMIP5 improves the ISM simulation. In the process, we intend to evaluate the role of air-sea coupling in the simulation of the ISOs of ISM and the monsoon low-pressure systems (LPS). The rest of the paper is arranged as follows: the details of the RCMs and the experiments are presented in Section 2, followed by the results in Section 3 with a discussion of the implication of the results in Section 4 preceding the summary and conclusions in Section 5.

2. Models, Experimental Details, and Methods

We used coupled ocean-atmosphere RCM and atmosphere-only RCM as dynamical downscaling tools centered over the Indian subcontinent. The Regional Spectral Model (RSM; Juang & Kanamitsu, 1994; Misra et al., 2017) coupled with the Regional Ocean Modeling System (ROMS, Haidvogel et al., 2000; Shchepetkin & McWilliams, 2005), hereafter referred to as CRSM is used for coupled ocean-atmosphere simulations and RSM forced by prescribed SST from CCSM4 (hereafter referred as URSM) is used for the atmosphere-only simulations. Both URSM and CRSM have been widely used for regional climate studies in India and other parts of the world (Ham et al., 2016; Karmakar & Misra, 2020; Li et al., 2012; Li & Misra, 2014; Misra & Jayasankar, 2022; Misra et al., 2017, 2018).

2.1. Uncoupled Regional Climate Model

The URSM is a primitive equation atmospheric model in which the spectral method is used to estimate the advective derivatives (Juang & Kanamitsu, 1994). A semi-implicit scheme for time integration is used in the URSM.

Table 1
A Comparison of the ISM Studies Which Evaluated the Impact of the Air-Sea Coupling in Regional Climate Models

References	Atmospheric model (horizontal resolution)	Oceanic model (horizontal resolution)	Air-sea coupling interval	Lateral boundary forcings for the atmosphere	Lateral boundary forcings for ocean	SST boundary condition for stand-alone atmospheric model integration	Length of model integration	Use of flux correction
Ratnam et al. (2009)	RegCM3 (60 km)	ROMSv2.2 (60 km)	1 day	NCEP-NCAR reanalysis	Monthly Levitus climatology	Interpolated from weekly OISST (Reynolds & Smith, 1994)	Seasonal runs for 4 years (1997, 1998, 2002, 2003) from 1 May to 30 September	Levitus Climatology is used for surface salinity
Samala et al. (2013)	WRFv2.2 (30 km)	ROMSv2.2 (10 km)	6 hr	NCEP-NCAR reanalysis	Monthly Levitus climatology	Interpolated from weekly OISST (Reynolds & Smith, 1994)	Seasonal runs for 8 years (2000–2007)	Levitus Climatology is used for surface salinity
Umakant and Kesarkar (2018)	RegCM4.4 (50 km)	Slab ocean model with a thickness of 50 m	At every atmospheric model time step	ERA-15 reanalysis	n/a	1. Interpolated from weekly OISST 2. SST prescribed at a daily interval from coupled model experiment	13-year continuous run from 1 January 2000	Q-flux correction is applied
Di Sante et al. (2019)	RegCM4 (50 km)	MITgcm in its regional configuration (18 km)	3 hr	ERA-Interim reanalysis	ORAP5 ocean reanalysis	1. ERA-Interim SSTs 2. SST prescribed from coupled integration at a daily interval	30-year continuous run from 1979 to 2008	None
Mishra et al., 2021	RegCM4 (50 km)	MITgcm in its regional configuration (20 km)	n/a	ERA-Interim reanalysis	ORAP5 ocean reanalysis	Interpolated from weekly OISST	21 years from 1995 to 2015	n/a
Kumar, Mishra, et al., 2022 (Regional earth system model)	REMO (25 km)	MPIOM coupled with HAMOCC (variable resolution from 10 km along the coast to 100 km in the southern seas)	3 hr	ERA-Interim reanalysis	n/a	ERA-Interim SST	38-year run from 1980 to 2017	None
This study	RSM (20 km)	ROMSv2.2 (20 km)	1 hr	CCSM4 historical integration for CMIP5	CCSM4 historical integration for CMIP5	Daily SST from CCSM4 historical integration for CMIP5	20-year run from 1 January 1986	None

The URSM contains 28 irregular terrain-following sigma levels, and the top-level is approximately at 2 hPa. From the suite of physics schemes, URSM is configured with the Relaxed Arakawa Schubert scheme (Moorthi & Suarez, 1992) for deep convective parameterization and Tiedtke (1983) scheme for shallow convection. In addition, URSM uses Zhao and Carr (1997) prognostic cloud scheme, which represents cloud liquid water and cloud ice specifically in the prognostic equations of the model. The Hong and Pan (1996) scheme is used for the planetary boundary layer turbulence, the Noah land surface model (Ek et al., 2003) for the land surface processes, Chou and Lee (1996) scheme for the longwave radiation, and Chou and Suarez (1994) scheme for the shortwave radiation. Furthermore, URSM uses the scale selective bias correction (Kanamaru & Kanamitsu, 2007) to prevent synoptic-scale drift during the RCM integration. The sponge zone's width is set to 16 grid points at the edges of the model boundaries. Earlier studies have indicated that these model physics schemes are the most suitable combination for simulating the ISM (e.g., Misra et al., 2017, 2022).

2.2. Coupled Regional Climate Model

The CRSM is a coupled regional ocean-atmosphere model. The RSM is the atmospheric component of the CRSM and is configured identically to URSM (i.e., physics and dynamics are the same). The oceanic component of CRSM is ROMS and which is a free-surface ocean model. The split explicit time-stepping method is employed to solve the equations. The stretched terrain-following coordinates with 30 levels are used in the vertical discretization of the model. In this study, ROMS utilized the second-order biharmonic horizontal diffusion (Ezer et al., 2002). The vertical mixing parameterization is a nonlocal K-profile closure scheme introduced by Large et al. (1994). The K-profile approach includes both the top and bottom oceanic boundary layers. An efficient dual Message Passing Interface parallelization approach is used to couple RSM and ROMS and the coupling interval is 1-hr (Li et al., 2012). Both the RSM and ROMS are configured on the same grid of 20-km resolution, which helps to avoid the flux coupler with the direct exchange of atmospheric fluxes and SST between two model components as the model integration progresses every hour, without interpolation. Besides, no flux adjustment is applied in the CRSM integration.

2.3. Experimental Details

Any RCM relies on the large-scale initial conditions and time-varying lateral boundary forcing, commonly derived from a coarse-resolution global GCM. Previous studies show that NCAR's Community Climate System Model version 4 (hereafter CCSM4; Gent et al., 2011) is one of the better performing models in the CMIP5. It has the demonstrable skill to simulate the present-day ISM and its variability (Jayasankar et al., 2015, 2018; Mishra et al., 2018). In this study, for both the URSM and CRSM, the initial and the lateral boundary forcing for both the atmosphere and the ocean are taken from the CMIP5 historical coupled simulation of the CCSM4 model. The RSM (in both URSM and CRSM) is forced at its lateral boundaries with time-varying lateral boundary forcing of the three-dimensional atmospheric variables at 6-hourly intervals. In the URSM, the SST is prescribed at a daily interval from the historical simulation of CCSM4. The initial and the lateral boundary forcing for ROMS are taken from the oceanic component of CCSM4 (i.e., Parallel Ocean Program version 2) and is prescribed to ROMS at monthly interval. The atmospheric component of CCSM4 has $1.25° \times 0.9375°$ resolution grids, whereas the ocean component has nominal $1° \times 1°$ grids with increased resolution in the tropics.

Both URSM and CRSM are configured at 20-km resolution and have a domain span from 10.46°S to 37.94°N (278 grid points) and 50.04° to 110.4°E (325 grid points), which includes the sponge zone of 16 grid points. This study carried out two sets of 20-year (1986–2005) regional climate simulations: (a) URSM and (b) CRSM present-day simulations. Both the RCMs were driven by the historical simulations of CCSM4. Both RCMs generate output data at 1-hourly temporal resolution. The validation data sets used to validate simulated fields of both the CRSM and URSM are discussed in Text S1 in Supporting Information S1. Furthermore, Supporting Information S1 includes the methodology to extract the ISO signals (Text S2) and the method to track the LPS (Text S3).

3. Results

3.1. Mean Features of ISM

Taylor diagram is used to compare the spatial patterns of 20-year June-July-August-September (hereafter JJAS) climatology in URSM, CRSM, and the parent model (i.e., CCSM4) with observation/reanalysis (Figure 1). Taylor

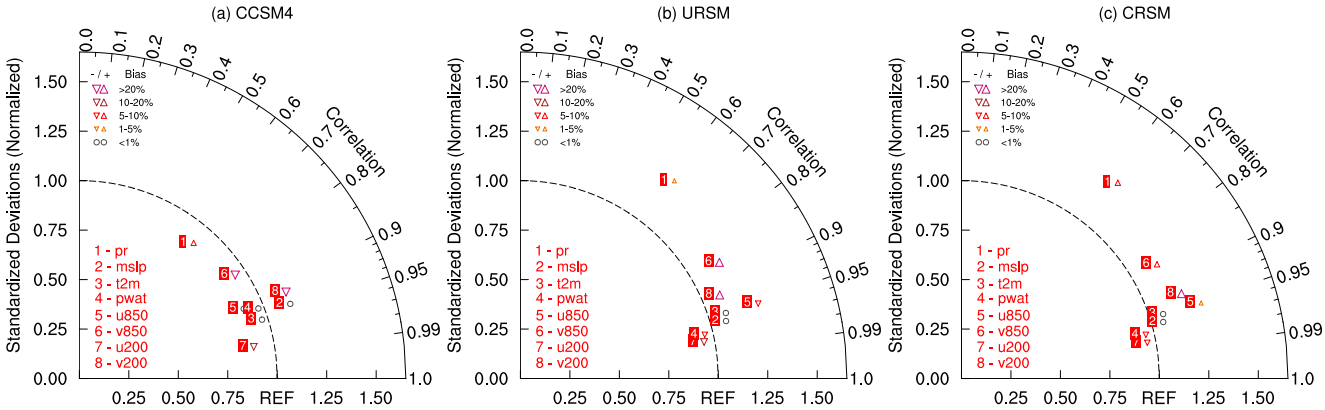

Figure 1. Taylor diagram of 20-year June–September mean climatology of rainfall (1, pr), mean sea level pressure (2, mslp), 2-m air temperature (3, t2m), precipitable water (4, pwat), 850-hPa zonal wind (5, u850), 200-hPa zonal wind (7, u200), 850-hPa meridional wind (6, v850), and 200-hPa meridional wind (8, v200) for (a) CCSM4, (b) URSM and (c) CRSM with respect to India Meteorological Department (for rainfall) and ERA5 for the rest of the variables. The percentage bias for each variable is represented using different symbols along with the variable numbers.

statistics are estimated over India (only land region) for mean rainfall (pr), precipitable water vapor (pwat), 2-m air temperature (t2m), mean sea level pressure (mslp), zonal wind at 850 hPa (u850), 200 hPa (u200) and meridional winds at 850 hPa (v850), 200 hPa (v200) with respect to IMERG (for rainfall) and fifth-generation ECMWF reanalysis (ERA5; Hersbach et al., 2020) for the other variables. Taylor diagram consists of (a) spatial pattern correlation coefficient (PCC), (b) ratio between the standardized variances of the model and the observation, and the (c) percentage bias for any field X between model (X_{model}) and the observation ($X_{\text{observation}}$), defined as;

$$\text{Percentage bias of Variable } X = \frac{(X_{\text{model}} - X_{\text{observation}}) \times 100}{X_{\text{observation}}} \quad (1)$$

The CCSM4 model exhibits reasonable skill in simulating the JJAS climatology of pwat, mslp, t2m, u850, and u200 except for v850 in comparison to ERA5 (Figure 1a). CCSM4 shows that the PCC is greater than 0.9 and the ratio of the standardized variance is between 0.84 and 1.08 for pwat, mslp, t2m, u850, u200, and v200. The PCC of v850 (0.84) is slightly less than other variables and has a higher percentage bias of −140.0%. However, both the URSM (Figure 1b) and CRSM (Figure 1c) show slightly improved PCC (>0.96) than CCSM4 (Figure 1a) for v850. The standardized variances of most variables in URSM and CRSM are closer to observations, that is, the ratio of standardized variance is closer to "REF" in the Taylor diagram. The percentage bias of v850 is 77.7% in URSM, which is further improved to 6.16% in CRSM.

We analyzed the simulated June–September mean climatological winds at 850 and 200 hPa with respect to the ERA5 (Figure S1 in Supporting Information S1). At 850 hPa, the weaker bias of the Somali Jet present over the Arabian Sea in both the URSM and the CRSM is a manifestation of a similar bias in CCSM4 (Figures S1a–S1c in Supporting Information S1). However, the weaker bias of the southwesterlies over the Indian Ocean and the cyclonic flow over the monsoon trough region in CCSM4 are significantly ameliorated in the RCMs.

At 200 hPa, we found that the CCSM4 largely underestimates the tropical easterly jet (TEJ), while both RCMs outperform their parent model in reducing the magnitude of this bias (Figures S1d–S1f in Supporting Information S1) with CRSM reducing the weak tropical easterly jet bias slightly more than URSM (Figures S1d–S1f in Supporting Information S1). Furthermore, the 500-hPa geopotential heights also indicate a reduction of the positive bias across the regional domain in the RCMs relative to CCSM4 (Figures S1g–S1i in Supporting Information S1).

The distribution of rainfall across the equatorial Indian Ocean, northeastern regions, orographic rainfall over the Western Ghats and adjacent oceans, core monsoon zone, and the foothills of the Himalayas is one of the most distinctive features of ISM. From the Taylor diagram, the PCC for rainfall (over Indian landmass based on India Meteorological Department observed rainfall) for CCSM4, URSM, and CRSM are 0.65, 0.60, and 0.62, respectively. Similarly, the ratio of the standardized variances for rainfall in CCSM4, URSM, and CRSM are 0.71, 1.08, and 1.08, and the percentage biases are 11.92%, 6.85%, and 13.15%, respectively. This suggests that the URSM has less rainfall bias than the CCSM4 over the Indian subcontinent, whereas the

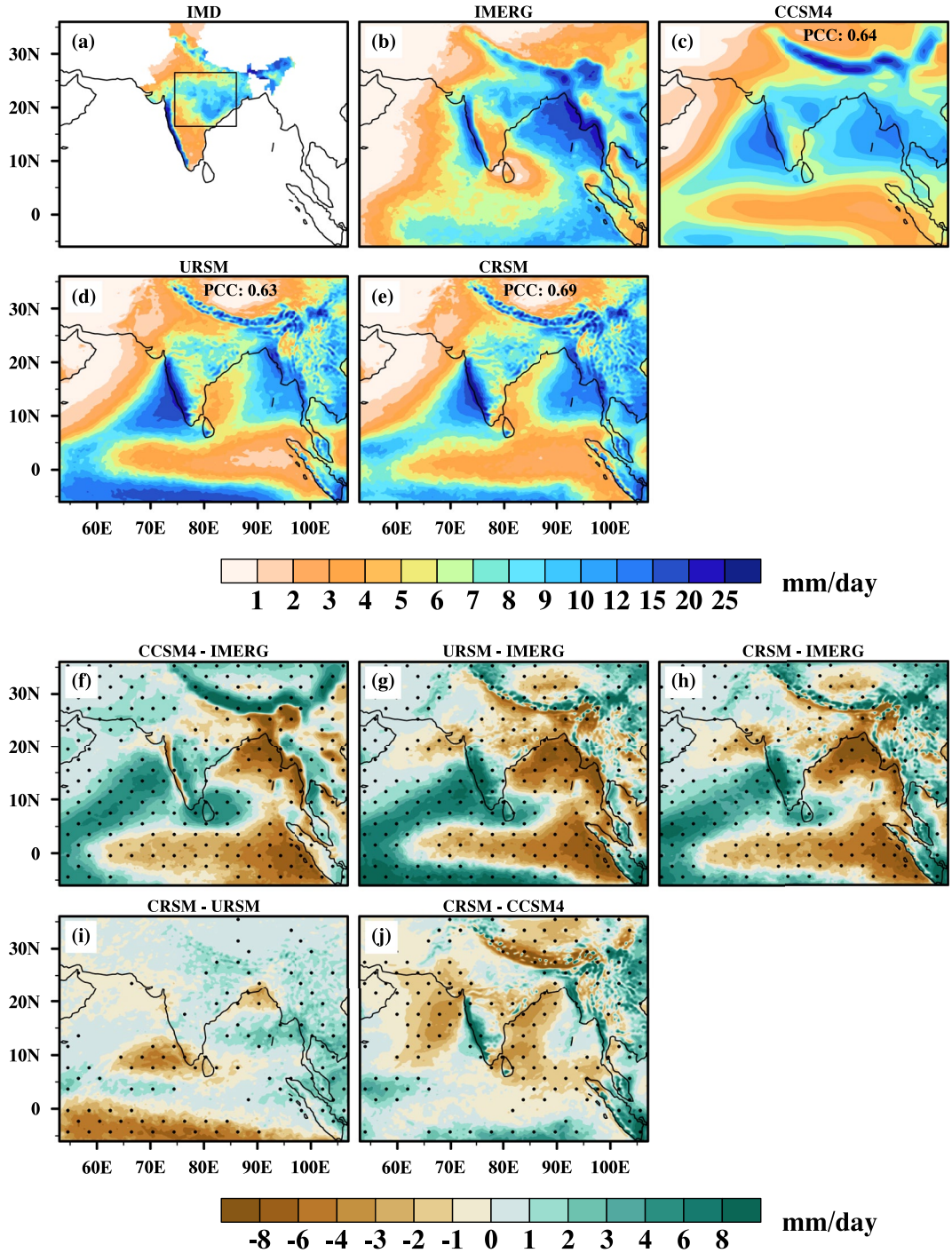

Figure 2. Spatial distribution of 20-year June–September mean rainfall (mm/day) climatology from (a) India Meteorological Department (IMD), (b) IMERG, (c) CCSM4, (d) URSM, and (e) CRSM. The climatological mean bias of (f) CCSM4, (g) URSM, and (h) CRSM with respect to IMERG observation. The corresponding seasonal climatological difference between (i) CRSM and URSM and (j) CRSM and CCSM4. Pattern correlation coefficient (PCC) between the IMERG and the models for pan ISM region (5°S–38°N and 55°–100°E) is given in the panel (c, d, and e) Climatological differences significant at a 5% level ($p = 0.05$) are stippled in panel (f–j). The Central India region referenced in the text is outlined in panel (a).

CRSM has slightly more bias than the CCSM4. Also, both the RCMs have strong wet bias over the Western Ghats (Figures 2g and 2h) which also contributes to this percentage bias. However, the sample sizes for the statistics generated in the Taylor diagram are vastly different given the contrast in the grid resolutions of CCSM4 and the RCMs. Therefore, even comparable statistics in the Taylor diagram between CCSM4 and the

RCMs should be noted as an improvement. In summary, the statistics from the Taylor diagram show a clear improvement in URSM and CRSM relative to CCSM4. However, the differences between URSM and CRSM are at best subtle.

Figures 2a and 2b show the observed 20-year (1986–2005) JJAS climatology from India Meteorological Department (1986–2005) and 20-year (2001–2020) JJAS climatology from IMERG, respectively. The corresponding climatology from CCSM4, URSM, and CRSM in Figures 2c–2e show the relative maximum ISM rainfall over Western Ghats, Central and Northeastern India, Arakan Mountain of Myanmar as in the observations (Figures 2a and 2b). The systematic bias of the JJAS rainfall from the models (Figures 2f–2h) shows dry bias over the equatorial Indian Ocean and the BoB most prominently, which is further exacerbated in the RCMs relative to CCSM4. The dry bias found over Central India is also slightly larger in the RCMs compared to CCSM4. However, in URSM, this dry bias is more severe compared to CRSM, suggesting a possible ocean rectification effect in the latter. Both URSM and CRSM overestimate the orographic rainfall and adjacent oceans primarily because of the terrain following the sigma vertical coordinate of RSM (i.e., the atmospheric component of the RCMs) which exacerbates the discontinuity of the orography in the upper troposphere that initiates unwarranted gravity waves (Gallus Jr., 2000; Zangl, 2002). By considering the mean climatology spatial pattern over Central India (16.5°–26.5°N, 74.5°–86.5°E, marked in Figure 2a), the RMSE is nearly comparable in CRSM (1.89 mm/day) with URSM (2.07 mm/day). However, URSM (bias: −11.14 mm/day, Figure 2g) exhibits a large dry bias over the Central Indian region, that is considerably reduced in CRSM (bias: −2.45 mm/day, Figure 2h). This dry rainfall bias over Central India is a common problem for many stand-alone atmosphere RCMs. Earlier studies have shown that this dry bias over Central India can be minimized by introducing the air-sea coupling in the regional model (e.g., Hari Prasad et al., 2021; Samanta et al., 2018), which is consistent with our results.

When we examine the differences between CRSM and CCSM4 (Figure 2j), we find that the CRSM overestimates the orographic rainfall over the Western Ghats and underestimates the rainfall over the Arabian Sea (AS) and the western BoB. But overall, across the pan ISM region (5°S–38°N and 55°–100°E) CRSM at PCC = 0.69 and RMSE = 3.5 mm/day capture the spatial heterogeneity of the ISM rainfall only marginally better than URSM with PCC = 0.62 and RMSE = 4 mm/day.

3.2. Mean Seasonal Cycle of Rainfall

Mean seasonal cycles were extracted using harmonic analysis (Murakami et al., 1986) to understand the seasonal variation of rainfall simulated by the dynamically downscaled models. The seasonal cycle of ISM rainfall is defined as the sum of the first four harmonics from the area-averaged rainfall climatology over all India (e.g., Jayasankar et al., 2015). The mean seasonal cycle of rainfall for the Indian land region from India Meteorological Department observation, CCSM4, URSM, and CRSM is shown in Figure S2 in Supporting Information S1. CCSM4 overestimates the seasonal cycle of rainfall throughout the year (0.45–1.2 mm/day), and the maximum overestimation (0.94–1.2 mm/day) is during the October to December period. A large wet bias found over the Western Ghat regions (Figures 2g and 2h) is partially responsible for this overestimation of area-averaged rainfall over Indian landmass in both the RCMs. However, this wet bias of the area-averaged rainfall time series is somewhat reduced because of the URSM's significant dry bias across Central India. Both the URSM (systematic error range is −0.3 to 0.21 mm/day) and CRSM (−0.15 to 0.34 mm/day) exhibit improvement over their parent model (0.47–0.56 mm/day) during the April–June period while the differences amongst the RCMs are comparably modest. Also, during the months of April–June, monthly mean rainfall from the RCMs falls within the observed standard deviation in contrast to CCSM4. But like CCSM4, the mean rainfall peak of ISM is overestimated in RCMs with nearly a delay of 1 week. The rainfall peak is, however, delayed by 3 days in CCSM4 (Figure S2 in Supporting Information S1).

3.3. Mean Summer Monsoon SST and Latent Heat Flux

Figure 3 exhibits the spatial patterns of mean JJAS SST from observation (OISST), URSM (SST prescribed from CCSM4), and CRSM, along with the corresponding mean bias of URSM and CRSM with respect to OISST. Both the URSM and CRSM have slightly warmer SST than observation, with the climatological mean SST bias over the domain being 0.62 and 0.33°C, respectively. The PCC for the entire domain for URSM and CRSM is 0.85 and 0.83, respectively. Similarly, the RMSE for CRSM at 0.53°C is slightly better than the URSM at 0.70°C. In comparison with OISST, CRSM shows slightly colder SST over the northern AS and over western BoB (Figure 3e). Indian Ocean warm pool (IOWP; 2°S–5°N and 65°−80°E; SST >28°C; Vinayachandran & Shetye, 1991) significantly influence the seasonal variability of the ISM (e.g., Kim et al., 2012). The RCM simulated location of IOWP is in

10.1029/2022EA002733

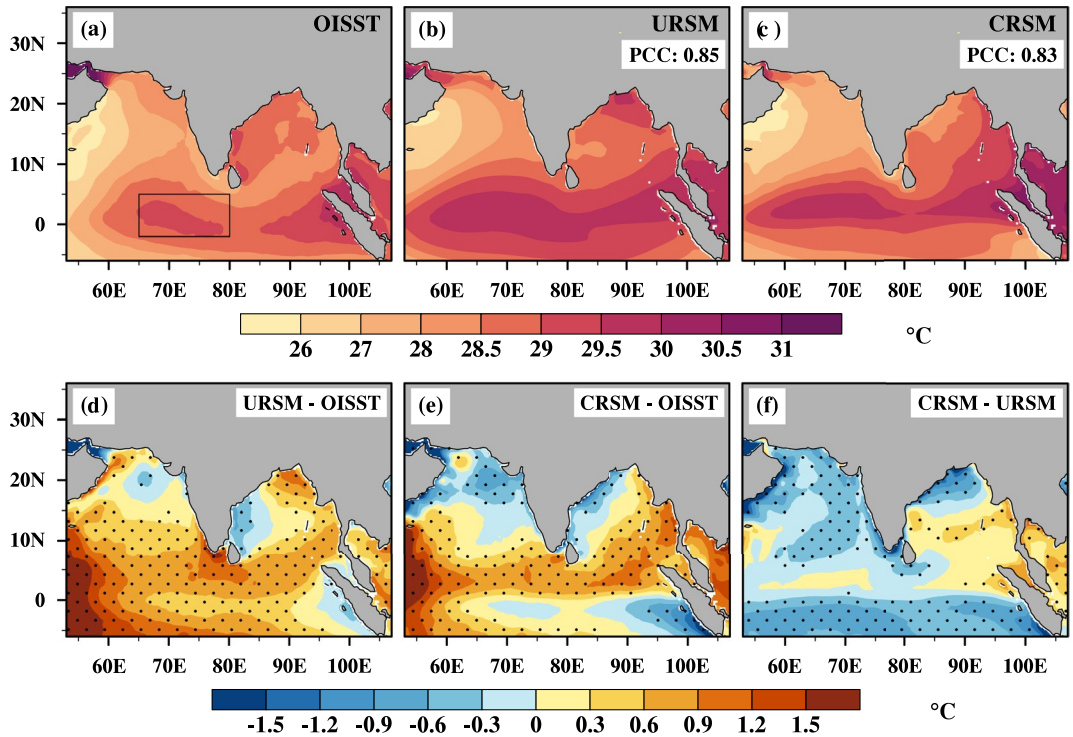

Figure 3. Spatial distribution of 20-year JJAS climatological mean SST (°C) from (a) OISST, (b) URSM, and (c) CRSM. The June–September climatological mean bias of (d) URSM, and (e) CRSM with respect to OISST observation. (f) The corresponding difference between the CRSM and URSM seasonal climatology. Pattern correlation coefficient (PCC) between the OISST and the models for the entire ocean is given in panel (b and c). Climatological differences significant at a 5% level ($p = 0.05$) are stippled in panel (d-f). The Indian Ocean Warm Pool (IOWP) region referenced in the text is outlined in panel (a).

good agreement with the OISST; however, the IOWP SST simulated by CRSM (RMSE = 0.64°C) is slightly better than the URSM (RMSE = 0.89°C). The URSM displays a warm bias of 0.5–1°C over a wider region in the equatorial Indian Ocean, which is significantly narrowed and reduced in the CRSM (Figure 3f). This improvement of CRSM over URSM in the tropical Indian Ocean is another indication of the potential ocean rectification in the former.

Tomita and Kubota (2004) from their observational study indicate that latent heat flux is a major part of the net heat flux in the northern Indian Ocean during ISM. Therefore, we examined in Figure 4 the mean JJAS latent heat flux simulated by the CCSM4, URSM, and CRSM, and compared them with OAFlux. In OAFlux (Figure 4a), the magnitude of the latent heat flux is larger (>130 W/m^2) over some parts of the AS and the BoB compared to the IOWP region (<120 W/m^2). CCSM4 largely underestimated the latent heat flux over both the AS and equatorial Indian Ocean (Figures 4b and 4e). URSM overestimated the latent heat flux south of the equator, over the AS, and northern regions of BoB (Figures 4c and 4f). The systematic bias between URSM and OAFlux shows an overestimation over head BoB and southern AS region (Figure 4f). However, the systematic bias between the CRSM and OAFlux (Figure 4g) shows an underestimation of about 10–20 W/m^2 over northern parts of AS and BoB. The major difference between the URSM and CRSM mean latent heat flux pattern is the significant overestimation of flux by the URSM over the AS, head BoB, and south of the equator (Figure 4h). The corresponding PCC (percentage bias) in URSM and CRSM is 0.72 (19.7%) and 0.71 (2.5%) over the AS region (5°–20°N and 65°−75°E), 0.58 (16.3%) and 0.77 (15.9%) over the BoB region (5°–20°N and 85°−95°E) with respect to OAFlux, respectively. Also, the spatial distributions of latent heat flux simulated by the models are, however, closely related to their simulated rainfall pattern (Figure 2).

The CRSM exhibits reasonable skill in simulating the spatial distribution of observed mean summer monsoon mixed layer depth (MLD) features, such as deeper MLD over the western AS and comparatively shallower MLD over the BoB (e.g., Misra et al., 2022). However, CRSM underestimates the magnitude of the MLD in most of the areas and overestimates over certain areas of the northern BoB and certain areas of southern AS (Figure S3 in Supporting Information S1). The air-sea coupling in CRSM likely improved the representation of ocean stratification which manifested with reduced biases in the SST and latent heat flux, especially over the northern BoB,

10.1029/2022EA002733

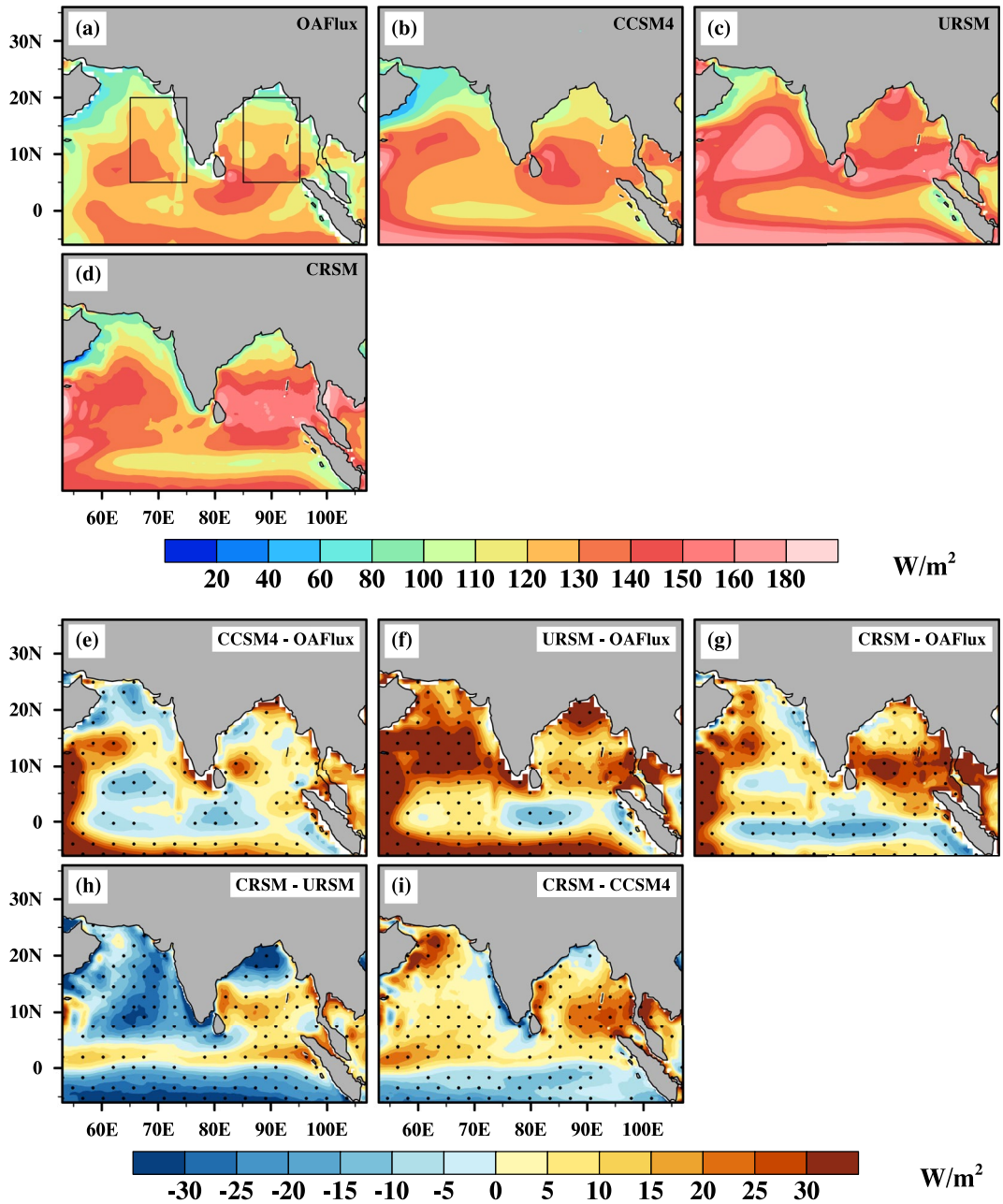

Figure 4. Spatial distribution of 20-year JJAS climatological mean latent heat flux (W/m^2) from (a) OAFlux, (b) CCSM4, (c) URSM, and (d) CRSM. The corresponding seasonal climatological mean bias of (e) CCSM4, (f) URSM, and (g) CRSM with respect to OAFlux. The June-September climatological difference of latent heat flux between (h) CRSM and URSM and (i) CRSM and CCSM4. Climatological differences significant at a 5% level ($p = 0.05$) are stippled in panel (e–i). The regions of the Arabian Sea (AS) and Bay of Bengal (BoB) referenced in the text are outlined in (a).

and the equatorial Indian Ocean relative to URSM. But cold SST bias (from −0.3 to −0.9°C) and underestimation of the latent heat flux over northwestern BOB in CRSM is also coincident with positive bias (1–10 m) in the MLD, suggesting the potential role of atmospheric processes in the SST bias.

3.4. Intraseasonal Oscillations of Rainfall

The irregular wet and dry spells of ISM rainfall is caused by the propagating ISOs (10–20 days and 20–70 days). The intraseasonal migration of the intertropical convergence zone is responsible for these wet and dry spells

(Sikka & Gadgil, 1980). Figure S4 in Supporting Information S1 shows the spectrum of area-averaged rainfall over Central India (marked in Figure 2a) from India Meteorological Department observations, CCSM4, URSM, and CRSM. The India Meteorological Department rainfall observations show a peak periodicity at ∼50 days which is simulated by all the models (Figure S4 in Supporting Information S1). The phase composite diagrams of HFISO from IMERG rainfall observations (Figure 5a) derived from Multi-channel Singular Spectrum Analysis (MSSA) exhibit strong positive anomalies in the BoB, Central India, and northern Western Ghats in the first four phases (i.e., wet spell), which is replaced by negative anomalies in the next four phases (i.e., dry spell). It is evident from the corresponding composites of the wet and the dry spells of the ISM simulated by both URSM (Figure 5b) and CRSM (Figure 5c), that they can reproduce the observed spatial distributions of the HFISO. Nonetheless, the high magnitudes of the observed HFISO rainfall anomalies over the BoB are not seen in either URSM or CRSM. For example, in Phases 2–3 and 6–7, strong HFISO anomalies found over the northwestern BoB and which extend all the way to Central India in URSM (Figure 5b) are comparatively weak in northeastern BoB (Figure 5c). In Phases 2–4 and 6–8 of the observed HFISO (Figure 5a), the positive and the negative anomalies are observed over eastern AS adjacent to the northern Western Ghats, respectively. The location of these anomalies is shifted to central-Western Ghats and further inland in URSM and CRSM, and the magnitude is slightly overestimated in URSM (Figure 5b) compared to CRSM (Figure 5c). The wet and the dry phase composites of HFISO derived from the CCSM4 (i.e., parent GCM) also shows the observed spatial patterns of rainfall HFISO anomalies (Figure S5a in Supporting Information S1). Figure S5a in Supporting Information S1 shows positive rainfall anomalies in northern BoB in Phase 1, which starts moving inland in Phase 2, while anomalies are mostly found over Central India in Phase 3 and Phase 4 is a transition phase to the dry spell.

The magnitudes of the observed LFISO rainfall anomalies (Figure 6a) are stronger than HFISO anomalies (Figure 5a). Unlike HFISO (Figure 5a), LFISO anomalies in Figure 6a span across the continental region. Both URSM (Figure 6b) and CRSM (Figure 6c) perform reasonably in simulating the spatial characteristics of the eight phases of LFISO features over both land and Ocean. However, the RCMs underestimate the LFISO rainfall anomalies. Furthermore, both RCMs overestimate the LFISO anomalies over the Western Ghats region and the anomalies are slightly shifted inland. Additionally, the negative anomalies in Phase 1 and positive anomalies in Phase 5 over northern BoB are absent in both URSM and CRSM and are located further northward unlike observations. Additionally, the strong positive and negative anomalies in Phases 3/4 and 7/8 over northern BoB and along coastal Arakan mountains are missing in both URSM and CRSM simulations, respectively. Similarly, the wet and the dry phase composites of LFISO derived from the CCSM4 (i.e., parent GCM) show the observed spatial patterns of rainfall anomalies (Figure S5b in Supporting Information S1). The CRSM exhibits slight improvement in positive (negative) LFISO anomalies over BoB in Phase 2 (Phase 6) compared to URSM, which potentially points to the ocean rectification impact of the CRSM.

We investigated the propagation characteristics of HFISO and LFISO anomalies over the BoB (zonally averaged over 85° to 95°E) and AS (zonally averaged over 65°–75°E) using the phase-latitude Hovemöller diagrams (Figures 7a–7l and Figures S6a–S6d in Supporting Information S1). These diagrams show the northward propagation of the rainfall anomalies both in the observations and in the RCMs, with the northward propagation from the equatorial latitudes to the foothills of the Himalayas around ∼22°N and beyond. We further estimated the phase speed (± standard error, i.e., $\sigma/\sqrt{N}$, where σ is the standard deviation and N is the number of samples) of the northward propagating HFISO and LFISO in both the ocean basins (AS and BoB) for IMERG, CCSM4, URSM and CRSM (Table 2). The ISO-filtered rainfall anomalies over AS have a higher propagation speed than the BoB, which is consistent with the results of Karmakar and Misra (2020). This is verified by all models including CCSM4 (Table 2). Furthermore, all models like the observations show that the standard error of the phase speeds of the ISO is higher in AS than over BoB (Table 2). The relative differences in the phase speeds of the ISO between the models and in relation to observations are small (Table 2). The results from this study suggest that the role of air-sea coupling in CRSM did not significantly affect the propagation characteristics of either HFISO or LFISO. This leads us to conclude that the impact of air-sea coupling in the CRSM to simulate the ISO features is relatively small at least in the case of downscaling CCSM4, which has a robust ISO signal (Figures S5 and S6 in Supporting Information S1). However, the significance of air-sea coupling in the successful simulation of the ISO cannot be undermined given that CCSM4 is a coupled ocean-atmosphere GCM. Similarly, Mishra, Kumar, et al. (2022) found that the improvement in the propagation characteristic of ISO simulated by the regional ESM was minimal compared to the stand-alone atmospheric RCM. They attributed this feature to the prominent role of atmospheric internal dynamics of the coupled system and the SST bias in the regional ESM.

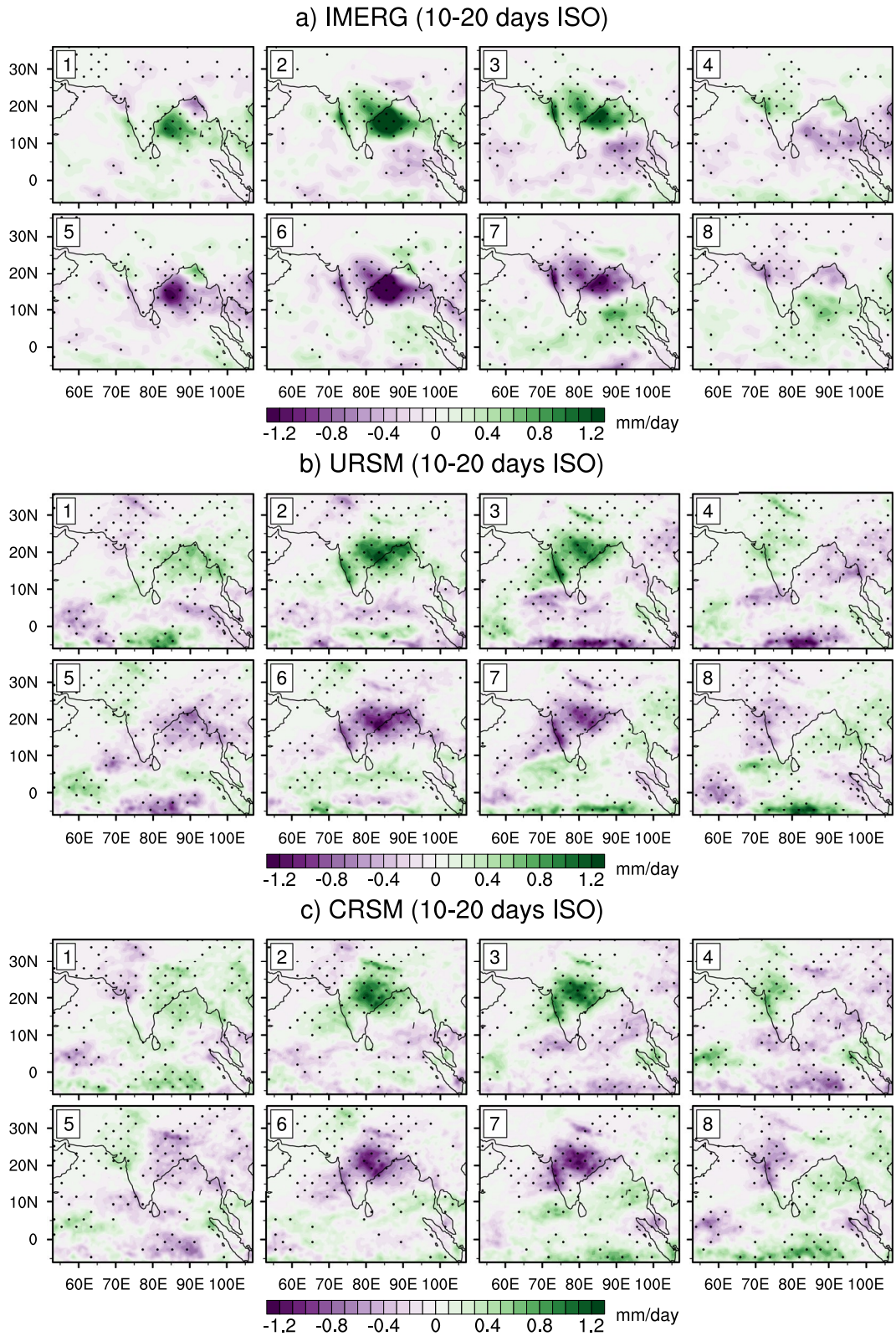

Figure 5. The climatological phase composites of 10–20-day ISO filtered daily rainfall (mm/day) anomalies based on the April to October, from (a) IMERG, (b) URSM, (c) CRSM. The numbers (top left corner) in each sub-figure denote the phase numbers. Stippling indicates a 95% confidence level estimated using the bootstrap method with 1,000 samples.

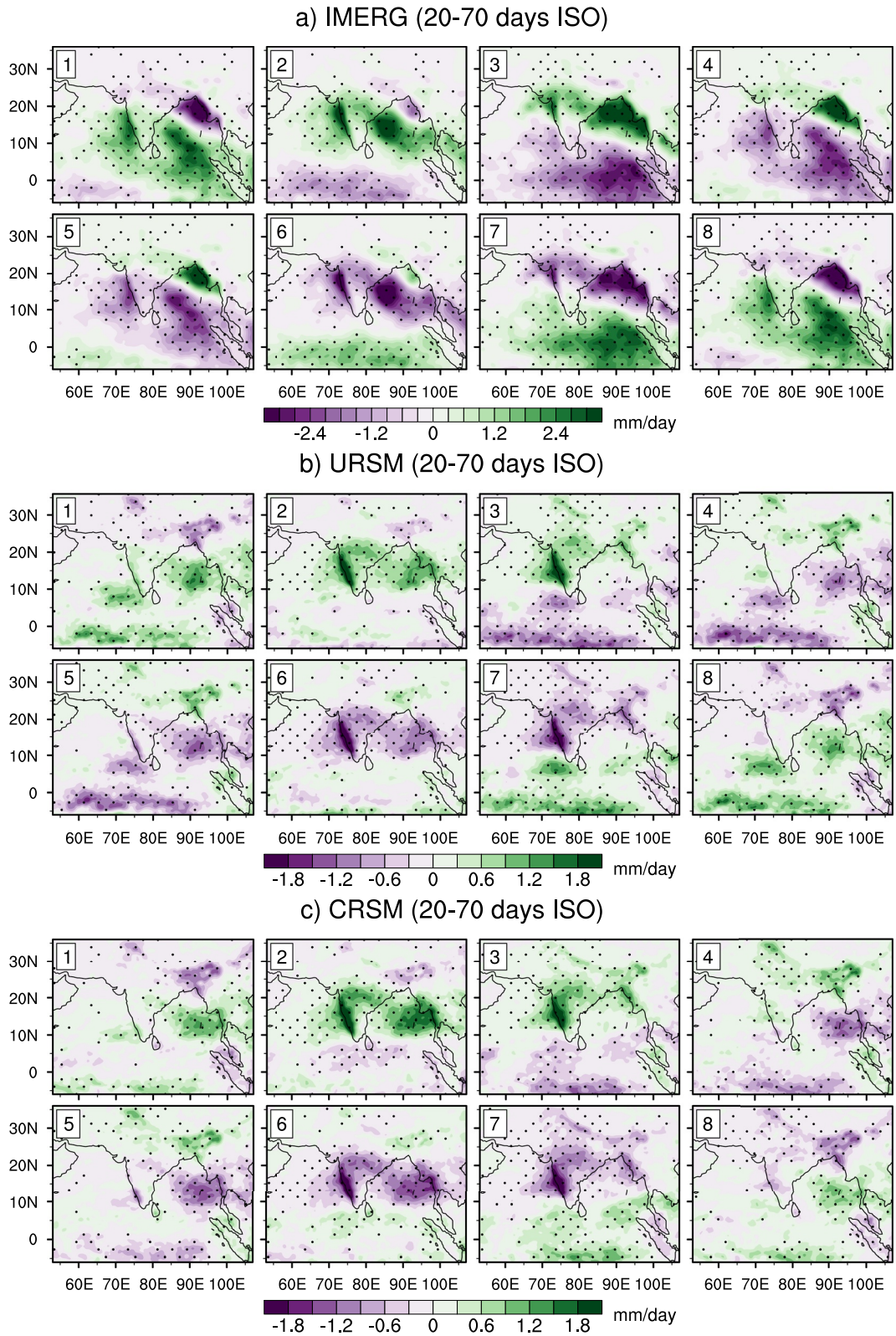

Figure 6. The climatological phase composites of 20–70-day ISO filtered daily rainfall (mm/day) anomalies based on the April to October from (a) IMERG, (b) URSM, (c) CRSM. The numbers (top left corner) in each sub-figure denote the phase numbers. Stippling indicates a 95% confidence level estimated using the bootstrap method with 1,000 samples.

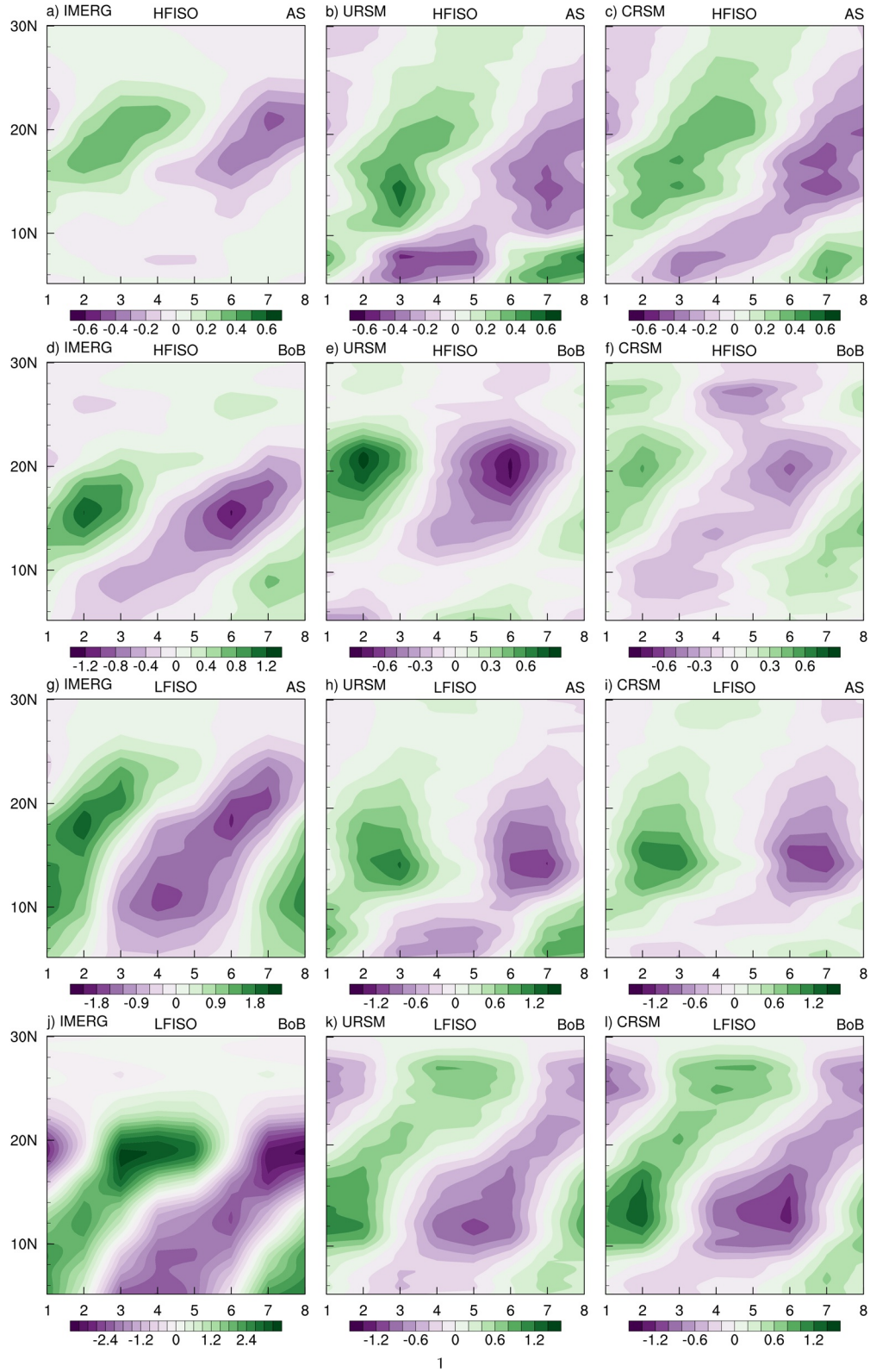

Figure 7. Phase-latitude diagrams of 10–20-day (HFISO, (a–f) and 20–70-day (LFISO, (g–l) ISO-filtered rainfall (mm/day) anomalies averaged over AS longitudes (65°−75°E) and BoB longitudes (75°−85°E) during April–October for IMERG (a, d, g, and j), URSM (b, e, h, and k), and CRSM (c, f, i, and l).

Table 2
Mean Phase Speed and Standard Error (in °/day) of Northward Propagation of HFISO and LFISO Filtered Rainfall Anomalies Over the Arabian Sea (AS) and the Bay of Bengal (BoB) Longitudes Between the Latitudes of 5° and 30°N During the Convective Events in IMERG, CCSM4, URSM, and CRSM

	ISO	AS (∘/day)	BoB (∘/day)
IMERG	HFISO	1.24 ± 0.09	0.95 ± 0.06
	LFISO	1.37 ± 0.07	0.99 ± 0.04
CCSM4	HFISO	1.31 ± 0.21	1.02 ± 0.12
	LFISO	1.29 ± 0.08	0.92 ± 0.06
URSM	HFISO	1.13 ± 0.12	0.98 ± 0.11
	LFISO	1.11 ± 0.11	0.97 ± 0.09
CRSM	HFISO	1.19 ± 0.14	1.01 ± 0.11
	LFISO	0.94 ± 0.10	0.83 ± 0.05

HFISO often propagates northwestward from the BoB to northwestern India (Chen & Chen, 1993; Karmakar et al., 2017a). We investigated the westward propagation of HFISO by using the phase-longitude Hovemöller diagrams of ISO-filtered rainfall anomalies averaged over the Central Indian latitudes (15°–20°N) and which are shown in Figure 8. These Hovemöller diagrams clearly show the westward propagation of the HFISO rainfall anomalies both in the IMERG observations, CCSM4 and in the RCMs. The anomalies are stronger in IMERG than in the model simulations, and the CCSM4 anomalies are slightly stronger than in the RCMs. It is found that the anomalies in the observation and the models propagate from around ∼100° to ∼70°E.

3.5. Association of Intraseasonal Oscillations of Rainfall With Low-Pressure Systems

LPS are the major rain-bearing systems during the monsoon season, and most of these synoptic-scale systems form over north BoB and move northwestward into the Indian landmass. During ISM, the majority of the LPS originate from a region of BoB where the MLD is very shallow. The salinity is also low in this area due to the freshwater availability from the river discharges and

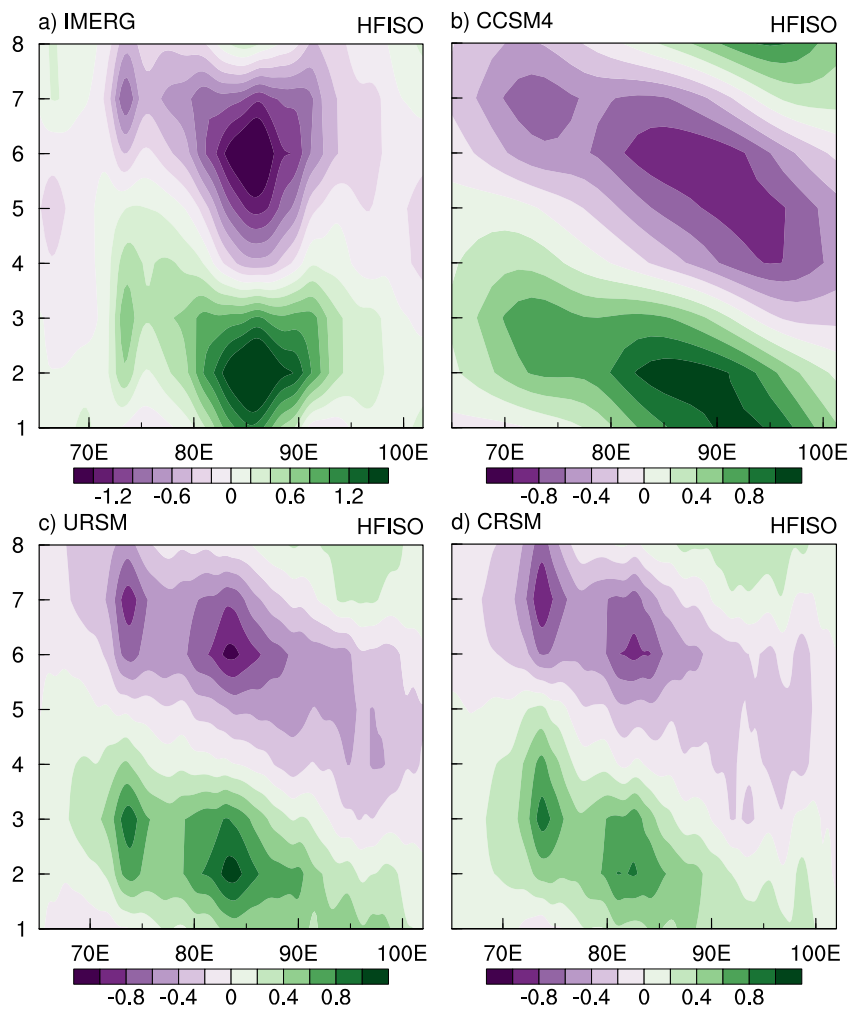

Figure 8. Phase-longitude diagrams of 10–20-day ISO-filtered (HFISO) rainfall (mm/day) anomalies averaged over Central Indian latitudes (15°–20°N) during April to October for (a) IMERG, (b) CCSM, (c) URSM, and (d) CRSM.

10.1029/2022EA002733

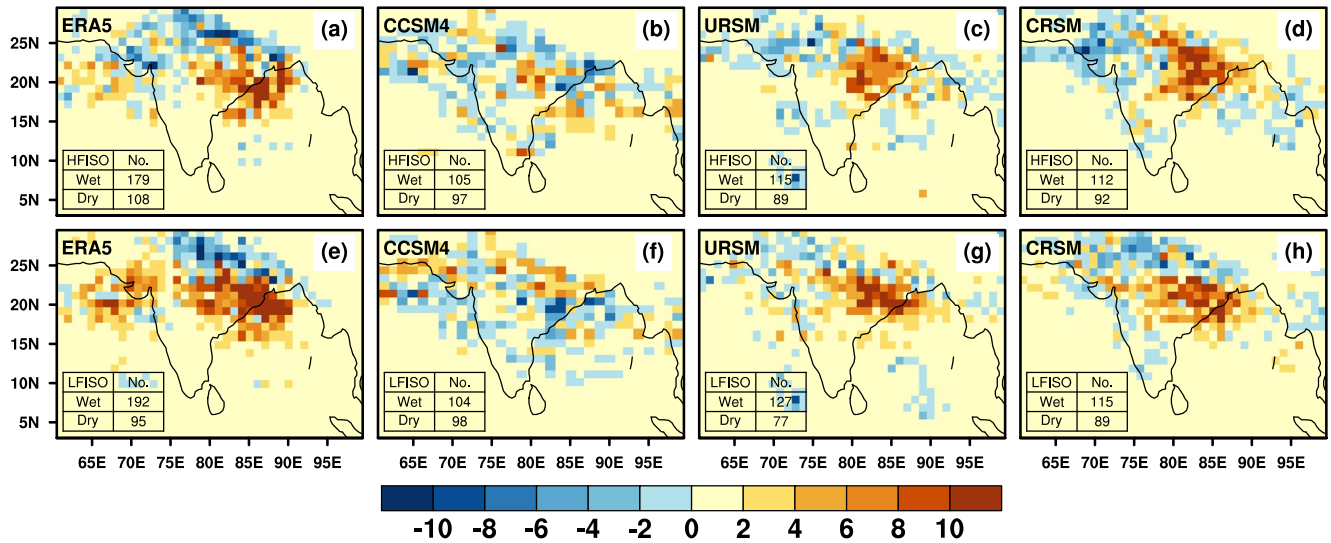

Figure 9. Difference between the wet (i.e., days when monsoon low-pressure systems are in Phase 1 to 4) and dry (i.e., days when low-pressure systems is in Phase 5 to 8) track density (i.e., no. of tracks per 1 × 1 grid cell) of the low-pressure systems formed throughout June–September for ERA5 (a, e), CCSM4 (b, f), URSM (c, g) and CRSM (d, h). The first row (a, b, c, and d) is for the 10–20-day HFISO and the second row (e, f, g, and h) is for the 20–70-day LFISO. The tracks were considered only for the strong HFISO/LFISO days. Track density is generated from data available at 6-hourly intervals. The inset table in (a–h) provides the total number (No.) of LPS during the wet and dry phases of HFISO/LFISO.

this mostly helps to form warm SST anomalies on ISO timescales (Goswami et al., 2016). Srivastava et al. (2017) found that the improved air-sea interaction in their CGCM helped to reproduce the observed LPS modulation by ISO and its associated rainfall over Central India. In CRSM, the simulated mixed layer is deeper over BoB along with a cold SST bias, which may not be the most conducive condition for LPS genesis. SST biases at intraseasonal time scales may be caused by the biases in the mixed layer and heat fluxes associated with the ISO, which may modulate convection (Goswami et al., 2016). Krishnamurthy and Ajayamohan (2010) and Karmakar et al. (2021) highlighted that the number of LPSs formed during the wet phases is higher than the dry phases. Karmakar et al. (2021) showed that the genesis of monsoon lows (weaker LPS) is insensitive to the phase of ISO, whereas, the stronger depressions show a clear preference for genesis in wet relative to dry spells of the LFISO. In addition, Krishnamurthy and Ajayamohan (2010) suggest that LPS formed during wet phases of the ISO move more northwestward than those that form during dry phases. We estimated the total number of LPS tracks using the TempestExtremes tracking algorithm over a 20-year (1986–2005) period, from June to September across all simulation datasets used in this study. The ERA5 data set shows 287 LPS tracks (Figure S7a in Supporting Information S1), whereas both URSM (Figure S7c in Supporting Information S1) and CRSM (Figure S7d in Supporting Information S1) underestimated the number of tracks, with both showing 204 tracks over the 20-year period. Out of 287 LPS tracks in ERA5, 181 tracks are of monsoon lows, and 106 tracks are of monsoon depressions (i.e., strong LPS having MSLP closed contour of magnitude greater than or equal to 400-Pa and have maximum surface wind speed greater than 8.5 m/s, Figure S8a in Supporting Information S1). Though, both the URSM and the CRSM have 204 tracks, their number of lows and depressions are slightly different. The URSM and CRSM simulations show 114 and 117 monsoon lows, and 90 (Figure S8b in Supporting Information S1) and 87 (Figure S8c in Supporting Information S1) monsoon depressions, respectively. We also estimated the total number of tracks in CCSM4 (202 tracks: Figure S7b in Supporting Information S1). There are some subtle but important differences that the models display with respect to ERA5, like the excessive density over western India and AS in CCSM4 (Figure S7b in Supporting Information S1), underestimation of the density in the northern BoB in RCMs (Figures S7c and S7d in Supporting Information S1) and higher density of LPS in peninsular India in all models.

It is found that the number of LPS tracks in the wet ISO phase is more than that of dry phases in the ERA5 reanalysis (Figures 9a and 9e and Figure S9 in Supporting Information S1), which is like earlier studies (Goswami et al., 2003; Karmakar et al., 2021; Krishnamurthy & Ajayamohan, 2010). The reduction of LPS in the dry relative to wet phases of HFISO in ERA5 is ∼39% (Figure 9a) while in LFISO it is ∼50.5% (Figure 9e). However, in CCSM4 the contrast in the track density of LPS formed during the wet and the dry phases of HFISO (Figure 9b) and LFISO (Figure 9f) is 7.6% and ∼5.7%, respectively. In contrast, URSM displays a reduction of track density

in the dry phases of the HFISO of 22.6% (Figure 9c) and for LFISO at 39.4% (Figure 9g) relative to the corresponding wet phases. Similarly, the intraseasonal contrast in the track density in CRSM in Figures 9d and 9h amount to 17.8% and 22.6% reduction in the dry phases of HFISO and LFISO relative to the corresponding wet phases, respectively. These results suggest the value addition of the RCMs with respect to the driving GCM. However, we observe that the LPS's track density variations between URSM and CRSM at the intraseasonal scales are comparable with some spatial differences. For example, the reduction in HFISO/LFISO track density over the northern regions of India is slightly better in CRSM than in the URSM. Similarly, the increase of track density over northwestern BoB and east Central India is slightly better in CRSM than in URSM. Overall, notwithstanding these subtle differences, the results from URSM and CRSM suggest that the impact of air-sea coupling in the CRSM in simulating the monsoon LPS and their association with the ISO of the ISM is relatively small.

4. Discussion

The evidence from the analysis of the model integrations suggests a clear benefit of downscaling CCSM4 at ∼1° grid resolution to 20 km grid using either URSM or CRSM. These results are noticeable in the seasonal mean fields of upper air (e.g., pwat, winds at 200 and 850 hPa), surface variables (e.g., MSLP, 2-m air temperature, rainfall), and in the intraseasonal variability of the LPS. Here, we have compared the URSM and CRSM simulated mean monsoon features. The mean Somali jet and TEJ simulated by CRSM have a slight improvement over URSM. Furthermore, SST and latent heat flux simulated by the CRSM shows an overall improvement over URSM. The differences that are most prominent are the reduction of the SST bias in the IOWP region in CRSM relative to URSM (i.e., the prescribed SST for URSM is from CCSM4). The impact of this ocean rectification effect manifests in the reduction of the mean dry bias of rainfall over Central India in CRSM relative to URSM and CCSM4. However, the differences between the CRSM and URSM at ISO timescales are weak and, in many instances, indistinguishable. For example, both URSM and CRSM simulate similar propagation characteristics of the LFISO that verify reasonably with observations.

Overall, do these results mean that air-sea coupling is not a significant process in ISM, contrary to many earlier studies? Our emphatic answer is no. Indeed, air-sea coupling is significant for ISM and its ISOs. After all, CCSM4 is a coupled ocean-atmosphere model. What this study is suggesting is that ocean-atmosphere coupling in the RCM may not always drastically improve the simulation of ISOs of the ISM. For example, Karmakar and Misra (2020) indicated that the differential speed of propagation of the ISO between the AS and BoB is a result of the anomalous intraseasonal winds advecting across climatological humidity gradients in the lower troposphere. This feature of the ISO had no connection with air-sea coupling at the high-resolution local scales (Karmakar & Misra, 2020). Therefore, if these upper air features are prevalent in the large-scale, an uncoupled RCM like URSM could simulate the ISO under reasonable SST forcing similar to a coupled RCM like CRSM. There are some notable differences in the mean fields between CRSM and URSM, but they are not reflected in the differences in the variability at the intraseasonal or even at the synoptic scales (LPS) of ISM in a significant manner. In this study, by comparing CRSM and URSM forced by an imperfect CCSM4 at the lateral boundaries and at the surface with SST from CCSM4 for the latter, we are able to isolate the role of air-sea coupling to examine the 'added value' of CRSM over URSM.

5. Summary and Conclusions

This study investigated the fidelity of the high-resolution (20-km) 20-year integration of CRSM and URSM driven by CCSM4 in simulating the observed features of the ISM. The results show that the URSM and CRSM perform better than CCSM4 in capturing the climatological characteristics of the ISM. When we examine climatological rainfall over India, the differences amongst the models are small with the PCC being 0.64, 0.61, 0.62, the ratio of the standardized variances being 0.84, 1.21, and 1.21, and the percentage bias being 9.43%, 3.58%, 9.67% for CCSM4, URSM, and CRSM, respectively. However, owing to the higher resolution of the RCMs compared to CCSM4, the gradients of the mean rainfall especially along the orographic regions within the domain are sharper and appear more realistic in the former. Furthermore, the CRSM simulates the spatial heterogeneity of the ISM rainfall better with the CRSM outperforming the URSM, especially over the ocean. The mean seasonal cycle of rainfall over India (area averaged over land) simulated by both URSM and CRSM is comparable with the observation and shows a marginal improvement over the CCSM4. The CRSM (RMSE = 0.64°C) simulated the IOWP SST more realistically than the CCSM4 (RMSE = 0.89°C). The CCSM4 displays a warm bias of

0.5–1°C over a broad area in the equatorial Indian Ocean which is significantly reduced to a narrower latitude band in the CRSM. Additionally, in comparison to its parent model, URSM and CRSM (and especially the latter) exhibit more comparable spatial patterns of 850 hPa winds, 200 hPa winds, SST, and latent heat flux with respect to observations. In comparison to URSM, the CRSM not only exhibits a modest improvement in simulating the spatial patterns of the mean climatology of the aforementioned variables, but it also considerably lessens the dry bias over Central India, the core region of the ISM.

At intraseasonal scales, our results show that in comparison to observations, both RCMs simulate the spatiotemporal evolution of HFISO and LFISO reasonably well. The phase-latitude Hovemöller diagrams showed reasonable phase speeds of the ISOs in the CCSM4 simulation as well. All models (RCMs and CCSM4) in the study like the IMERG rainfall observations display a differential meridional phase speed of the ISOs over AS and BoB with the ISOs being slower over the latter than over the former. However, the differences between CRSM and URSM at ISO timescales are weak. This result suggests a relative insensitivity of air-sea coupling in the RCM to simulate ISO features, which is also likely abetted by the realistic ISO signal simulated by the parent model (i.e., CCSM4). It should be however clear, that air-sea coupling could still be important to obtain reasonable ISO in the large-scale model given that CCSM4 is a CGCM.

LPS contributes a substantial percentage to the mean ISM rainfall. We attempted to elucidate the contrast of intraseasonal variability of LPS activity in URSM, CRSM, and CCSM4. The ERA5 has 287 LPS tracks over the 20-year period; however, CCSM4 has 202 tracks and both the URSM and CRSM display only 204 LPS tracks each. The observed LPS track density difference between the wet and the dry phases of strong HFISO and LFISO is captured in both URSM and CRSM. Even though there is no significant improvement in ISOs between the RCMs and the CCSM4, the value addition of downscaling is demonstrated in the simulated LPS and their association with the ISOs in the RCMs. The CCSM4 simulation is unable to produce the intraseasonal contrast in the LPS activity.

The relative insensitivity of air-sea coupling to ISO simulation in the RCM reported in this study holds some significance considering previous coupled RCM studies that seem to suggest otherwise. Although the benefits of air-sea coupling and potential ocean rectification effect in CRSM over URSM are clear over the mean ISM simulation. But as pointed out earlier, this is the first such study that cleanly isolates the role of air-sea coupling in an RCM that is not forced by "perfect" or observed surface and reanalysis lateral boundary conditions, which can influence the role of air-sea coupling. However, the results presented here could be model dependent and would need to be repeated by downscaling other CGCMs and with other physical parameterization schemes in the RCM. There is also sufficient scope for improving the CRSM simulations of this study. For instance, bias in the key rainfall regions (e.g., Western Ghats, BoB, Central India), underestimation of monsoon LPS, underestimation of the magnitude of TEJ, and strong underestimation of MLD in the tropical Indian Ocean are evident in the CRSM simulation. But the results of this study are an outcome of the 20-year integration of the RCM and although the modeling system is far from ergodic, it still serves to provide a robust result.

Data Availability Statement

The high-resolution daily IMERG rainfall data set used for the analysis in this study is available at https://gpm.nasa.gov/data (Huffman et al., 2019). The India Meteorological Department rainfall data set used for the analysis in this study is available at https://www.imdpune.gov.in/cmpg/Griddata/Rainfall_25_NetCDF.html (Pai et al., 2014). The hourly ERA5 data used for the analysis in this study is available at https://doi.org/10.24381/cds.adbb2d47 (Hersbach et al., 2020). The OISST version 2 data used for the analysis in this study is available at https://psl.noaa.gov/data/gridded/data.noaa.oisst.v2.highres.html (Huang et al., 2021). The OAFlux data used for the analysis in this study is available at https://rda.ucar.edu/datasets/ds260.1/ (Yu et al., 2008). The datasets from the CMIP5 CCSM4 model simulations can be accessed through the ESGF data portal at https://esgf-node.llnl.gov/search/cmip5/ (ESGF, 2021) and the Research Data Archive of CISL at https://rda.ucar.edu/datasets/ds316.0/ (NCAR, 2011). The URSM and CRSM simulation datasets for the analysis and to produce the figures in the paper are available at https://osf.io/u63wp/ (Jayasankar et al., 2022). To generate Figures 5–9, Table 2, Figures S5 and S6 in Supporting Information S1 we have used Multichannel Singular Spectrum Analysis (MSSA) using MATLAB version R2020a available via https://www.mathworks.com/products/matlab.html (MATLAB, 2020) under FSU license 731138. The tracks of the LPS are identified using the TempestExtremes algorithm and which is available at https://github.com/ClimateGlobalChange/tempestextremes (Ullrich and Zarzycki, 2017). All the

final figures were generated using NCAR Command Language v6.6.2 and which is available via http://dx.doi.org/10.5065/D6WD3XH5 (NCAR, 2019).

Acknowledgments
The present study is supported by NASA's Grants 80NSSC19K1199 and 80NSSC22K0595. The first author is thankful to S Vishnu, Meteo-France, Toulouse, France for guidance in using the TempestExtremes algorithm.

References

Ajay, P., Pathak, B., Solmon, F., Bhuyan, P. K., & Giorgi, F. (2019). Obtaining best parameterization scheme of RegCM 4.4 for aerosols and chemistry simulations over the CORDEX South Asia. *Climate Dynamics*, *53*(1), 329–352. https://doi.org/10.1007/s00382-018-4587-3

Befort, D. J., Leckebusch, G. C., & Cubasch, U. (2016). Intraseasonal variability of the Indian summer monsoon: Wet and dry events in COSMO-CLM. *Climate Dynamics*, *47*(7), 2635–2651. https://doi.org/10.1007/s00382-016-2989-7

Bhaskaran, B., Jones, R. G., Murphy, J. M., & Noguer, M. (1996). Simulations of the Indian summer monsoon using a nested regional climate model: Domain size experiments. *Climate Dynamics*, *12*(9), 573–587. https://doi.org/10.1007/BF00216267

Bhaskaran, B., Ramachandran, A., Jones, R., & Moufouma-Okia, W. I. S. S. N. (2012). Regional climate model applications on sub-regional scales over the Indian monsoon region: The role of domain size on downscaling uncertainty. *Journal of Geophysical Research*, *117*(D10), D10113. https://doi.org/10.1029/2012JD017956

Chen, T. C., & Chen, J. M. (1993). The 10–20-day mode of the 1979 Indian monsoon: Its relation with the time variation of monsoon rainfall. *Monthly Weather Review*, *121*(9), 2465–2482. https://doi.org/10.1175/1520-0493(1993)121%3C2465:TDMOTI%3E2.0.CO;2

Chen, X., Pauluis, O. M., & Zhang, F. (2018). Regional simulation of Indian summer monsoon intraseasonal oscillations at gray-zone resolution. *Atmospheric Chemistry and Physics*, *18*(2), 1003–1022. https://doi.org/10.5194/acp-18-1003-2018

Chou, M. D., & Lee, K. T. (1996). Parameterizations for the absorption of solar radiation by water vapor and ozone. *Journal of the Atmospheric Sciences*, *53*(8), 1203–1208. https://doi.org/10.1175/1520-0469(1996)053<1203:pftaos>2.0.co;2

Chou, M. D., & Suarez, M. J. (1994). An efficient thermal infrared radiation parameterization for use in general circulation models. *NASA Technical Memorandum NASA-TM-104606*, *3*, 98. Retrieved from https://ntrs.nasa.gov/archive/nasa/casi.ntrs.nasa.%20gov/19950009331.pdf

Dash, S. K., Shekhar, M. S., & Singh, G. P. (2006). Simulation of Indian summer monsoon circulation and rainfall using RegCM3. *Theoretical and Applied Climatology*, *86*(1), 161–172. https://doi.org/10.1007/s00704-006-0204-1

Di Sante, F., Coppola, E., Farneti, R., & Giorgi, F. (2019). Indian Summer Monsoon as simulated by the regional Earth system model RegCM-ES: The role of local air–sea interaction. *Climate Dynamics*, *53*(1), 759–778. https://doi.org/10.1007/s00382-019-04612-8

Ek, M. B., Mitchell, K. E., Lin, Y., Rogers, E., Grunmann, P., Koren, V., et al. (2003). Implementation of Noah land surface model advances in the National Centers for Environmental Prediction operational mesoscale Eta model. *Journal of Geophysical Research*, *108*(D22), 8851. https://doi.org/10.1029/2002JD003296

ESGF. (2021). CMIP5 datasets are available through the Earth System Grid Federation portals. [Dataset]. Retrieved from https://esgf-node.llnl.gov/search/cmip5/

Ezer, T., Arango, H., & Shchepetkin, A. F. (2002). Developments in terrain-following ocean models: Intercomparisons of numerical aspects. *Ocean Modelling*, *4*(3–4), 249–267. https://doi.org/10.1016/S1463-5003(02)00003-3

Fu, X., Wang, B., & Li, T. (2002). Impacts of air–sea coupling on the simulation of mean Asian summer monsoon in the ECHAM4 model. *Monthly Weather Review*, *130*(12), 2889–2904. https://doi.org/10.1175/1520-0493(2002)130%3C2889:IOASCO%3E2.0.CO;2

Gallus, A. W., Jr. (2000). The impact of step orography in the Eta model: Two contrasting examples. *Weather and Forecasting*, *15*(5), 630–639. https://doi.org/10.1175/1520-0434(2000)015%3C0630:TIOSOO%3E2.0.CO;2

Gent, P. R., Danabasoglu, G., Donner, L. J., Holland, M. M., Hunke, E. C., Jayne, S. R., et al. (2011). The Community Climate System Model, version 4. *Journal of Climate*, *24*(19), 4973–4991. https://doi.org/10.1175/2011JCLI4083.1

Goswami, B. N., Ajayamohan, R. S., Xavier, P. K., & Sengupta, D. (2003). Clustering of synoptic activity by Indian Summer Monsoon intraseasonal oscillations. *Geophysical Research Letters*, *30*(8), 1431. https://doi.org/10.1029/2002GL016734

Goswami, B. N., Rao, S. A., Sengupta, D., & Chakravorty, S. (2016). Monsoons to mixing in the Bay of Bengal: Multiscale air-sea interactions and monsoon predictability. *Oceanography*, *29*(2), 18–27. https://doi.org/10.5670/oceanog.2016.35

Haidvogel, D. B., Arango, H. G., Hedstrom, K., Beckmann, A., Malanotte-Rizzoli, P., & Shchepetkin, A. F. (2000). Model evaluation experiments in the North Atlantic Basin: Simulations in nonlinear terrain-following coordinates. *Dynamics of Atmospheres and Oceans*, *32*(3), 239–81. https://doi.org/10.1016/S0377-0265(00)00049-X

Ham, S., Yoshimura, K., & Li, H. (2016). Historical dynamical downscaling for East Asia with the atmosphere and ocean coupled regional model. *Journal of the Meteorological Society of Japan. Series II*, *94A*(0), 199–208. https://doi.org/10.2151/jmsj.2015-046

Hari Prasad, K. B. R. R., Ramu, D. A., Rao, S. A., Hameed, S. N., Samanta, D., & Srivastava, A. (2021). Reducing systematic biases over the Indian region in CFS V2 by dynamical downscaling. *Earth and Space Science*, *8*(6), e2020EA001507. https://doi.org/10.1029/2020ea001507

Hersbach, H., Bell, B., Berrisford, P., Hirahara, S., Horányi, A., Muñoz-Sabater, J., et al. (2020). The ERA5 global reanalysis. [Dataset]. Quarterly Journal of the Royal Meteorological Society, *146*(730), 1999–2049. https://doi.org/10.1002/qj.3803

Hong, S. Y., & Pan, H. L. (1996). Nonlocal boundary layer vertical diffusion in a medium-range forecast model. *Monthly Weather Review*, *124*(10), 2322–2339. https://doi.org/10.1175/1520-0493(1996)124%3C2322:NBLVDI%3E2.0.CO;2

Huang, B., Liu, C., Banzon, V., Freeman, E., Graham, G., Hankins, B., et al. (2021). Improvements of the daily optimum interpolation sea surface temperature (DOISST) version 2.1 [Dataset]. Journal of Climate, *34*, 2923–2939. https://doi.org/10.1175/JCLI-D-20-0166.1

Huffman, G. J., Stocker, E. F., Bolvin, D. T., Nelkin, E. J., & Tan, J. (2019). GPM IMERG final precipitation L3 half hourly 0.1 degree x 0.1 degree V06. [Dataset]. Goddard Earth Sciences Data and Information Services Center (GES DISC). https://doi.org/10.5067/GPM/IMERG/3B-HH/06

Jayasankar, C. B., Misra, V., & Karmakar, N. (2022). Datasets from regional atmospheric model simulations and regional coupled Ocean-atmospheric model simulations over India [Dataset]. OSF. https://doi.org/10.17605/OSF.IO/U63WP

Jayasankar, C. B., Rajendran, K., & Surendran, S. (2018). Monsoon climate change projection for the orographic west coast of India using high-resolution nested dynamical downscaling model. *Journal of Geophysical Research: Atmospheres*, *123*(15), 7821–7838. https://doi.org/10.1029/2018JD028677

Jayasankar, C. B., Surendran, S., & Rajendran, K. (2015). Robust signals of future projections of Indian summer monsoon rainfall by IPCC AR5 climate models: Role of seasonal cycle and interannual variability. *Geophysical Research Letters*, *42*(9), 3513–3520. https://doi.org/10.1002/2015GL063659

Ji, Y., & Vernekar, A. D. (1997). Simulation of the Asian summer monsoons of 1987 and 1988 with a regional model nested in a global GCM. *Journal of Climate*, *10*(8), 1965–1979. https://doi.org/10.1175/1520-0442(1997)010%3C1965:SOTASM%3E2.0.CO;2

Jiang, X., Li, T., & Wang, B. (2004). Structures and mechanisms of the northward propagating boreal summer intraseasonal oscillation. *Journal of Climate*, *17*(5), 1022–1039. https://doi.org/10.1175/1520-0442(2004)017<1022:samotn>2.0.co;2

Juang, H. M. H., & Kanamitsu, M. (1994). The NMC nested regional spectral model. *Monthly Weather Review*, *122*(1), 3–26. https://doi.org/10.1175/1520-0493(1994)122%3C0003:TNNRSM%3E2.0.CO;2
Kanamaru, H., & Kanamitsu, M. (2007). Scale-selective bias correction in a downscaling of global analysis using a regional model. *Monthly Weather Review*, *135*(2), 334–350. https://doi.org/10.1175/MWR3294.1
Karmakar, N., Boos, W. R., & Misra, V. (2021). Influence of intraseasonal variability on the development of monsoon depressions. *Geophysical Research Letters*, *48*(2), e2020GL090425. https://doi.org/10.1029/2020GL090425
Karmakar, N., Chakraborty, A., & Nanjundiah, R. S. (2017a). Space–time evolution of the low-and high-frequency intraseasonal modes of the Indian summer monsoon. *Monthly Weather Review*, *145*(2), 413–435. https://doi.org/10.1175/MWR-D-16-0075.1
Karmakar, N., & Misra, V. (2020). Differences in northward propagation of convection over the Arabian Sea and Bay of Bengal during boreal summer. *Journal of Geophysical Research: Atmospheres*, *125*(3), e2019JD031648. https://doi.org/10.1029/2019JD031648
Kim, S. T., Yu, J. Y., & Lu, M. M. (2012). The distinct behaviors of Pacific and Indian Ocean warm pool properties on seasonal and interannual time scales. *Journal of Geophysical Research*, *117*(D5), D05128. https://doi.org/10.1029/2011JD016557
Kitoh, A., & Arakawa, O. (1999). On overestimation of tropical precipitation by an atmospheric GCM with prescribed SST. *Geophysical Research Letters*, *26*(19), 2965–2968. https://doi.org/10.1029/1999GL900616
Krishnamurthy, V., & Ajayamohan, R. S. (2010). Composite structure of monsoon low pressure systems and its relation to Indian rainfall. *Journal of Climate*, *23*(16), 4285–4305. https://doi.org/10.1175/2010JCLI2953.1
Krishnamurthy, V., & Shukla, J. (2007). Intraseasonal and seasonally persisting patterns of Indian monsoon rainfall. *Journal of Climate*, *20*(1), 3–20. https://doi.org/10.1175/JCLI3981.1
Kumar, D., Rai, P., & Dimri, A. P. (2020). Investigating Indian summer monsoon in coupled regional land–atmosphere downscaling experiments using RegCM4. *Climate Dynamics*, *54*(5), 2959–2980. https://doi.org/10.1007/s00382-020-05151-3
Kumar, P., Mallick, S., Mishra, A. K., Dubey, A. K., Tiwari, G., Sein, D. V., et al. (2022). Regional Earth system model for CORDEX-South Asia: A comparative assessment of RESM and ESM over the tropical Indian Ocean. *International Journal of Climatology*, *42*(16), 9131–9149. https://doi.org/10.1002/joc.7806
Kumar, P., Mishra, A. K., Dubey, A. K., Javed, A., Saharwardi, M. S., Kumari, A., et al. (2022). Regional Earth system modelling framework for CORDEX-SA: An integrated model assessment for Indian summer monsoon rainfall. *Climate Dynamics*, *59*(7–8), 2409–2428. https://doi.org/10.1007/s00382-022-06217-0
Large, W. G., McWilliams, J. C., & Doney, S. C. (1994). Oceanic vertical mixing: A review and a model with a nonlocal boundary layer parameterization. *Reviews of Geophysics*, *32*(4), 363–403. https://doi.org/10.1029/94RG01872
Levine, R. C., Klingaman, N. P., Peatman, S. C., & Martin, G. M. (2021). Roles of air–sea coupling and horizontal resolution in the climate model simulation of Indian monsoon low pressure systems. *Climate Dynamics*, *56*(3), 1203–1226. https://doi.org/10.1007/s00382-020-05526-6
Li, H., Kanamitsu, M., & Hong, S. Y. (2012). California reanalysis downscaling at 10 km using an ocean-atmosphere coupled regional model system. *Journal of Geophysical Research*, *117*(D12), D12118. https://doi.org/10.1029/2011JD017372
Li, H., & Misra, V. (2014). Thirty-two-year ocean–atmosphere coupled downscaling of global reanalysis over the Intra-American Seas. *Climate Dynamics*, *43*(9–10), 2471–2489. https://doi.org/10.1007/s00382-014-2069-9
Lin, J. L., Weickman, K. M., Kiladis, G. N., Mapes, B. E., Schubert, S. D., Suarez, M. J., et al. (2008). Subseasonal variability associated with Asian summer monsoon simulated by 14 IPCC AR4 coupled GCMs. *Journal of Climate*, *21*(18), 4541–4567. https://doi.org/10.1175/2008JCLI1816.1
Lucas-Picher, P., Christensen, J. H., Saeed, F., Kumar, P., Asharaf, S., Ahrens, B., et al. (2011). Can regional climate models represent the Indian monsoon? *Journal of Hydrometeorology*, *12*(5), 849–868. https://doi.org/10.1175/2011JHM1327.1
Maharana, P., Kumar, D., Das, S., & Tiwari, P. R. (2021). Present and future changes in precipitation characteristics during Indian summer monsoon in CORDEX-CORE simulations. *International Journal of Climatology*, *41*(3), 2137–2153. https://doi.org/10.1002/joc.6951
MATLAB. (2020). The MathWorks Inc. [Software]. Retrieved from https://www.mathworks.com/products/matlab.html
Maurya, R. K. S., Mohanty, M. R., Sinha, P., & Mohanty, U. C. (2020). Performance of hydrostatic and non-hydrostatic dynamical cores in RegCM4. 6 for Indian summer monsoon simulation. *Meteorological Applications*, *27*(3), e1915. https://doi.org/10.1002/met.1915
Mishra, A. K., Dwivedi, S., & Di Sante, F. (2021). Performance of the RegCM-MITgcm coupled regional model in simulating the Indian summer monsoon rainfall. *Pure and Applied Geophysics*, *178*(2), 603–617. https://doi.org/10.1007/s00024-020-02648-0
Mishra, A. K., & Dubey, A. K. (2021). Sensitivity of convective parameterization schemes in regional climate model: Precipitation extremes over India. *Theoretical and Applied Climatology*, *146*(1), 293–309. https://doi.org/10.1007/s00704-021-03714-w
Mishra, A. K., Dubey, A. K., & Dinesh, A. S. (2022). Diagnosing whether the increasing horizontal resolution of regional climate model inevitably capable of adding value: Investigation for Indian summer monsoon. *Climate Dynamics*, 1–21. https://doi.org/10.1007/s00382-022-06424-9
Mishra, A. K., Kumar, P., Dubey, A. K., Tiwari, G., & Sein, D. V. (2022). Impact of air-sea coupling on the simulation of Indian summer monsoon using a high-resolution Regional Earth System Model over CORDEX-SA. *Climate Dynamics*, *59*(9–10), 1–21. https://doi.org/10.1007/s00382-022-06249-6
Mishra, S. K., Sahany, S., Salunke, P., Kang, I. S., & Jain, S. (2018). Fidelity of CMIP5 multi-model mean in assessing Indian monsoon simulations. *Climate and Atmospheric Science*, *1*(1), 1–8. https://doi.org/10.1038/s41612-018-0049-1
Misra, V., & Jayasankar, C. B. (2022). A high resolution coupled ocean-atmosphere simulation of the regional climate over Central America. *Climate Dynamics*, *58*(11–12), 2981–3001. https://doi.org/10.1007/s00382-021-06083-2
Misra, V., Jayasankar, C. B., Mishra, A. K., Mitra, A., & Murugavel, P. (2022). Dynamic downscaling the South Asian summer monsoon from a global reanalysis using a regional coupled ocean-atmosphere model. *Journal of Geophysical Research: Atmospheres*, *127*(22). https://doi.org/10.1029/2022JD037490
Misra, V., Mishra, A., & Bhardwaj, A. (2017). High-resolution regional-coupled ocean–atmosphere simulation of the Indian summer monsoon. *International Journal of Climatology*, *37*(S1), 717–740. https://doi.org/10.1002/joc.5034
Misra, V., Mishra, A., & Bhardwaj, A. (2018). Simulation of the intraseasonal variations of the Indian summer monsoon in a regional coupled ocean–atmosphere model. *Journal of Climate*, *31*(8), 3167–3185. https://doi.org/10.1175/JCLI-D-17-0434.1
Moorthi, S., & Suarez, M. J. (1992). Relaxed Arakawa-Schubert. A parameterization of moist convection for general circulation models. *Monthly Weather Review*, *120*(6), 978–1002. https://doi.org/10.1175/1520-0493(1992)120%3C0978:RASAPO%3E2.0.CO;2
Murakami, T., Chen, L. X., Xie, A., & Shrestha, M. L. (1986). Eastward propagation of 30–60 day perturbations as revealed from outgoing longwave radiation data. *Journal of the Atmospheric Sciences*, *43*(10), 961–971. https://doi.org/10.1175/1520-0469(1986)043%3C0961:EPODPA%3E2.0.CO;2
NCAR. (2011). NCAR Community Earth System Model, [Dataset]. EaSM Project Dataset, Research Data Archive at the National Center for Atmospheric Research, Computational and Information Systems Laboratory. https://doi.org/10.5065/D6TH8JP5
NCAR. (2019). The NCAR Command Language (version 6.6.2). [Software]. UCAR/NCAR/CISL/TDD. https://doi.org/10.5065/D6WD3XH5

Pai, D. S., Rajeevan, M., Sreejith, O. P., Mukhopadhyay, B., & Satbha, N. S. (2014). Development of a new high spatial resolution (0.25× 0.25) long period (1901-2010) daily gridded rainfall data set over India and its comparison with existing data sets over the region. [Dataset]. Mausam, *65*, 1–18. https://doi.org/10.54302/mausam.v65i1.85

Pattnayak, K. C., Panda, S. K., Saraswat, V., & Dash, S. K. (2018). Assessment of two versions of regional climate model in simulating the Indian Summer Monsoon over South Asia CORDEX domain. *Climate Dynamics*, *50*(7), 3049–3061. https://doi.org/10.1007/s00382-017-3792-9

Peatman, S. C., & Klingaman, N. P. (2018). The Indian summer monsoon in MetUM-GOML2. 0: Effects of air-sea coupling and resolution. *Geoscientific Model Development*, *11*(11), 4693–4709. https://doi.org/10.5194/gmd-11-4693-2018

Rai, P. K., Singh, G. P., & Dash, S. K. (2020). Projected changes in extreme precipitation events over various subdivisions of India using RegCM4. *Climate Dynamics*, *54*(1–2), 247–272. https://doi.org/10.1007/s00382-019-04997-6

Rajendran, K., & Kitoh, A. (2006). Modulation of tropical intraseasonal oscillations by ocean–atmosphere coupling. *Journal of Climate*, *19*(3), 366–391. https://doi.org/10.1175/JCLI3638.1

Ratnam, J. V., Giorgi, F., Kaginalkar, A., & Cozzini, S. (2009). Simulation of the Indian monsoon using the RegCM3–ROMS regional coupled model. *Climate Dynamics*, *33*(1), 119–139. https://doi.org/10.1007/s00382-008-0433-3

Reynolds, R. W., & Smith, T. M. (1994). Improved global sea surface temperature analyses using optimum interpolation. *Journal of Climate*, *7*(6), 929–948. https://doi.org/10.1175/1520-0442(1994)007<0929:igssta>2.0.co;2

Samala, B. K., Banerjee, S., Kaginalkar, A., & Dalvi, M. (2013). Study of the Indian summer monsoon using WRF–ROMS regional coupled model simulations. *Atmospheric Science Letters*, *14*(1), 20–27. https://doi.org/10.1002/asl2.409

Samanta, D., Hameed, S. N., Jin, D., Thilakan, V., Ganai, M., Rao, S. A., & Deshpande, M. (2018). Impact of a narrow coastal Bay of Bengal Sea surface temperature front on an Indian summer monsoon simulation. *Scientific Reports*, *8*(1), 1–12. https://doi.org/10.1038/s41598-018-35735-3

Sharmila, S., Pillai, P. A., Joseph, S., Roxy, M., Krishna, R. P. M., Chattopadhyay, R., et al. (2013). Role of ocean–atmosphere interaction on northward propagation of Indian summer monsoon intra-seasonal oscillations (MISO). *Climate Dynamics*, *31*(5–6), 1651–1669. https://doi.org/10.1007/s00382-013-1854-1

Shchepetkin, A. F., & McWilliams, J. C. (2005). The regional oceanic modeling system (ROMS): A split-explicit, free-surface, topography-following-coordinate oceanic model. *Ocean Modelling*, *9*(4), 347–404. https://doi.org/10.1016/j.ocemod.2004.08.002

Sikka, D., & Gadgil, S. (1980). On the maximum cloud zone and the ITCZ over Indian, longitudes during the southwest monsoon. *Monthly Weather Review*, *108*(11), 1840–1853. https://doi.org/10.1175/1520-0493(1980)108%3C1840:OTMCZA%3E2.0.CO;2

Singh, S., Ghosh, S., Sahana, A. S., Vittal, H., & Karmakar, S. (2017). Do dynamic regional models add value to the global model projections of Indian monsoon? *Climate Dynamics*, *48*(3–4), 1375–1397. https://doi.org/10.1007/s00382-016-3147-y

Srivastava, A., Rao, S. A., Rao, D. N., George, G., & Pradhan, M. (2017). Structure, characteristics, and simulation of monsoon low-pressure systems in CFS v2 coupled model. *Journal of Geophysical Research: Oceans*, *122*(8), 6394–6415. https://doi.org/10.1002/2016jc012322

Tiedtke, M. (1983). The sensitivity of the time-mean large-scale flow to cumulus convection in the ECMWF model. In *Proceedings of ECMWF workshop on convective in large-scale models* (pp. 297–316). European Centre for Medium-Range Weather Forecasts.

Tomita, H., & Kubota, M. (2004). Variability of surface heat flux over the Indian Ocean. *Atmosphere-Ocean*, *43*(3), 183–199. https://doi.org/10.3137/ao.420303

Ullrich, P. A., & Zarzycki, C. M. (2017). TempestExtremes: A framework for scale-insensitive pointwise feature tracking on unstructured grids. [Software]. Geoscientific Model Development, *10*(3), 1069–1090. https://doi.org/10.5194/gmd-10-1069-2017

Umakanth, U., & Kesarkar, A. P. (2018). Performance evaluation of regional climate model to simulate sub-seasonal variability of Indian Summer Monsoon. *Climate Dynamics*, *50*(9), 3595–3612. https://doi.org/10.1007/s00382-017-3827-2

Umakanth, U., Kesarkar, A. P., Raju, A., & Vijaya Bhaskar Rao, S. (2016). Representation of monsoon intraseasonal oscillations in regional climate model: Sensitivity to convective physics. *Climate Dynamics*, *47*(3), 895–917. https://doi.org/10.1007/s00382-015-2878-5

Valdivieso, M., Peatman, S. C., & Klingaman, N. P. (2021). The influence of air-sea coupling on forecasts of the 2016 Indian summer monsoon and its intraseasonal variability. *Quarterly Journal of the Royal Meteorological Society*, *147*(734), 202–228. https://doi.org/10.1002/qj.3914

Vinayachandran, P. N., & Shetye, S. R. (1991). The warm pool in the Indian Ocean. *Proceedings of the Indian Academy of Sciences - Earth & Planetary Sciences*, *100*(2), 165–175. https://doi.org/10.1007/BF02839431

Wang, B., Ding, Q., Fu, X., Kang, I. S., Jin, K., Shukla, J., & Doblas-Reyes, F. (2005). Fundamental challenge in simulation and prediction of summer monsoon rainfall. *Geophysical Research Letters*, *32*(15), L15711. https://doi.org/10.1029/2005GL022734

Yu, L., Jin, X., & Weller, R. A. (2008). Multidecade global flux datasets from the Objectively Analyzed Air-sea fluxes (OAFlux) Project: Latent and sensible heat fluxes, ocean evaporation, and related surface meteorological variables. OA-2008-1. [Dataset]. Woods Hole Oceanographic Institution, 64. Retrieved from https://rda.ucar.edu/datasets/ds260.1/

Zangl, G. (2002). An improved method for computing horizontal diffusion in a sigma-coordinate model and its application to simulations over mountainous topography. *Monthly Weather Review*, *130*(5), 1423–1432. https://doi.org/10.1175/1520-0493(2002)130%3C1423:AIMFCH%3E2.0.CO;2

Zhao, Q., & Carr, F. H. (1997). A prognostic cloud scheme for operational NWP models. *Monthly Weather Review*, *125*(8), 1931–1953. https://doi.org/10.1175/1520-0493(1997)125%3C1931:APCSFO%3E2.0.CO;2

Zheng, Y., Waliser, D. E., Stern, W. F., & Jones, C. (2004). The role of coupled sea surface temperatures in the simulation of the tropical intra-seasonal oscillation. *Journal of Climate*, *17*(21), 4109–4134. https://doi.org/10.1175/JCLI3202.1

References From the Supporting Information

Ghil, M., Allen, M. R., Dettinger, M. D., Ide, K., Kondrashov, D., Mann, M. E., et al. (2002). Advanced spectral methods for climatic time series. *Reviews of Geophysics*, *40*(1), 31–341. https://doi.org/10.1029/2000RG000092

Karmakar, N., Chakraborty, A., & Nanjundiah, R. S. (2017b). Increased sporadic extremes decrease the intraseasonal variability in the Indian summer monsoon rainfall. *Scientific Reports*, *7*, 7824. https://doi.org/10.1038/s41598-017-07529-6

Karmakar, N., & Krishnamurti, T. N. (2018). Characteristics of northward propagating intraseasonal oscillation in the Indian summer monsoon. *Climate Dynamics*, *52*(3–4), 1903–1916. https://doi.org/10.1007/s00382-018-4268-2

Plaut, G., & Vautard, R. (1994). Spells of low-frequency oscillations and weather regimes in the Northern Hemisphere. *Journal of the Atmospheric Sciences*, *51*(2), 210–236. https://doi.org/10.1175/1520-0469(1994)051

Vishnu, S., Boos, W. R., Ullrich, P. A., & O'Brien, T. A. (2020). Assessing historical variability of South Asian monsoon lows and depressions with an optimized tracking algorithm. *Journal of Geophysical Research: Atmospheres*, *125*(15), e2020JD032977. https://doi.org/10.1029/2020JD032977

Wheeler, M. C., & Hendon, H. H. (2004). An all-season real-time multivariate MJO index: Development of an index for monitoring and prediction. *Monthly Weather Review*, *132*(8), 1917–1932. https://doi.org/10.1175/1520-0493(2004)132<1917:aarmmi>2.0.co;2